Geochemistry Geophysics Geosystems G3
AN ELECTRONIC JOURNAL OF THE EARTH SCIENCES
Published by AGU and the Geochemical Society

Article
Volume 10, Number 2
12 February 2009
Q02009, doi:10.1029/2008GC002141
ISSN: 1525-2027

Chemistry of hydrothermal plumes above submarine volcanoes of the Mariana Arc

Joseph A. Resing
Joint Institute for the Study of Atmosphere and Ocean, University of Washington, Pacific Marine Environmental Laboratory, NOAA, Seattle, Washington 98115-6349, USA (resing@u.washington.edu)

Edward T. Baker
Pacific Marine Environmental Laboratory, NOAA, Seattle, Washington 98115, USA

John E. Lupton
Pacific Marine Environmental Laboratory, NOAA, Newport, Oregon 97365, USA

Sharon L. Walker
Pacific Marine Environmental Laboratory, NOAA, Seattle, Washington 98115, USA

David A. Butterfield
Joint Institute for the Study of Atmosphere and Ocean, University of Washington, Pacific Marine Environmental Laboratory, NOAA, Seattle, Washington 98115-6349, USA

Gary J. Massoth
Institute of Geological and Nuclear Sciences, Ltd., P. O. Box 30368, Lower Hutt 5040, New Zealand

Now at Mass-Ex3 Consulting, LLC, 2100 Lake Washington Boulevard North, Renton, Washington 98056, USA

Ko-ichi Nakamura
Advanced Industrial Science and Technology, Tsukuba Central 1, Tsukuba, Ibaraki 305-8561, Japan

[1] Fifty submarine volcanoes of the Mariana Arc, covering 1200 km from 13.5°N to 23.2°N, were surveyed for hydrothermal activity. Of these 50 volcanoes, eight showed limited evidence of hydrothermal activity, while another 10 volcanoes displayed intense, chemically rich, hydrothermal plumes that allow detailed chemical characterization and insight into the hydrothermal activity forming the fluids that generate the plumes. The most active volcanoes exhibit a wide range of CO_2 to pH relationships, from the venting of acid-rich fluids, to CO_2-rich fluids, to fluids rich in alkalinity and CO_2. These pH-CO_2-alkalinity relationships are partially responsible for the wide range of Fe:Mn (3 to 32) observed at the different volcanoes. This chemical heterogeneity is further manifest in a wide range of CO_2:^{3}He (3×10^9 to 55×10^9), indicating that for all but one, >80% of the CO_2 venting from these volcanoes has a slab source. The helium, by contrast, has an upper mantle isotopic signature. The range of chemical conditions suggests that these volcanoes occupy various states of eruptive evolution ranging from ongoing magmatic activity to highly evolved hydrothermal systems.

Components: 11,200 words, 6 figures, 4 tables.

Keywords: hydrothermal; volcano; arc; geochemistry; erupt; plume.

Index Terms: 8427 Volcanology: Subaqueous volcanism; 8413 Volcanology: Subduction zone processes (1031, 3060, 3613, 8170); 4813 Oceanography: Biological and Chemical: Ecological prediction.

Received 1 July 2008; **Revised** 10 October 2008; **Accepted** 5 November 2008; **Published** 12 February 2009.

Resing, J. A., E. T. Baker, J. E. Lupton, S. L. Walker, D. A. Butterfield, G. J. Massoth, and K. Nakamura (2009), Chemistry of hydrothermal plumes above submarine volcanoes of the Mariana Arc, *Geochem. Geophys. Geosyst.*, *10*, Q02009, doi:10.1029/2008GC002141.

1. Introduction

[2] Recent studies of hydrothermal activity on submarine volcanoes along volcanic arcs reveal a great diversity of hydrothermal activity, resulting in a wide range of hydrothermal plume chemistry [e.g., *de Ronde et al.*, 2001; *Massoth et al.*, 2004; *de Ronde et al.*, 2007]. Volcanic arcs contain both subaerial and submarine volcanoes with 80% of the arc submarine volcanoes found along intraoceanic arcs [*de Ronde et al.*, 2003]. Subaerial arc volcanoes are well studied and characterized, while those in the submarine setting have only recently begun to receive attention. This recent attention reveals exciting new types of hydrothermal activity at sites like NW Eifuku [*Lupton et al.*, 2006], NW Rota-1 [*Embley et al.*, 2006; *Resing et al.*, 2007], and Suiyo Seamount [*Tsunogai et al.*, 1994]. In 1995 hydrothermal activity along arcs had been identified at only seven different sites [*Ishibashi and Urabe*, 1995]; however, since that time more than 30 active sites have been identified and sampled [*de Ronde et al.*, 2001; *de Ronde et al.*, 2007; *Massoth et al.*, 2007; *Embley et al.*, 2004]. Studies of the submarine hydrothermal systems along convergent margins offer insights on the effects of subducted crust on the products of arc volcanism and the flux of these products to the oceans. The shallow depths of many of these volcanoes result in the emplacement of their volcanic and hydrothermal products into the surface oceans where they influence surface ocean chemistry and productivity. While the length of the submarine intraoceanic arcs is only 10% of the global mid-ocean ridge system, the chemical observations made along the arcs to date [e.g., *Massoth et al.*, 2004; *Resing et al.*, 2007] show that the chemical enrichments in the arc hydrothermal plumes appear to be much greater than those in plumes found above mid-ocean ridges (MOR), suggesting that the flux of chemicals from submarine arcs may be significant on a global scale.

[3] We report here an almost comprehensive survey conducted in February 2003 of the submarine volcanoes located along more than 1200 km of the Mariana Arc from 13.5°N to 23.2°N. Prior to this survey, active hydrothermal discharge had been documented on six submarine volcanoes: Forecast Seamount [*Gamo et al.*, 1993], Kasuga-2 and Kasuga-3 [*McMurtry et al.*, 1993], Esmeralda Bank [*Stüben et al.*, 1992], Seamount X [*Masuda et al.*, 1994], and Toto [*Gamo et al.*, 2004] and was suspected on at least four more (Ruby, Ahyi, Fukujin, and Nikko) based on sightings of "discolored surface water" and seismic records. Those studies were conducted individually and not as part of a broad survey. During this survey we mapped and determined the status of hydrothermal activity at 50 submarine volcanoes using multibeam mapping and hydrothermal surveying techniques using 33 towed and 35 vertical conductivity-temperature-depth-optical (CTDO) hydrocasts. In addition, discrete samples were collected to chemically characterize the venting found (see auxiliary material for data from all CTD casts).[1] Repeat water column sampling and seafloor exploration of active volcanoes was carried out in both 2004 and 2006 [*Embley et al.*, 2007]. Between 2003 and 2006, 18 volcanoes exhibited some evidence of hydrothermal activity. Of the 18, 10 had easily identified, intense activity, another 6 had activity that had to be confirmed by chemical analyses, and 2 had very limited chemical evidence of hydrothermal activity. In this paper we describe the chemistry of the plumes found above these hydrothermally active volcanoes.

2. Regional Setting

[4] The Mariana Arc (Figure 1) is part of the Izu-Bonin-Mariana (IBM) arc system, which is an

[1] Auxiliary materials are available in the HTML. doi:10.1029/2008GC002141.

intraoceanic convergent margin that extends southward more than 2500 km from Japan to south of Guam. Along the IBM system, the Pacific Plate subducts beneath the Philippine plate and is the oldest subducting oceanic lithosphere on Earth. This results in a uniquely cold subduction zone with an extraordinarily deep penetration of the subducting slab into the mantle [*van der Hilst et al.*, 1991]. These factors suggest that the transport of elements from the slab into the overlying mantle is likely to be dominated by fluids [*Peacock*, 1990]. The volcanic activity along the arc results from the increased fertility of mantle materials due to the release of water from the subducting slab [*Peate and Pearce*, 1998]. The arc most closely approaches the back arc at the southern and northern ends of the arc, approaching to within 10 km of the back arc ridge at the southern end of the arc [*Martinez and Taylor*, 2003].

3. Methods

[5] Mariana Arc submarine volcanoes were surveyed using a Sea Bird 911 plus CTD (Conductivity, Temperature, Depth) augmented with a light scattering sensor (LSS, Seapoint Inc.) and an Oxidation Reduction Potential (ORP) sensor. Discrete water samples were collected using a rosette package with 21 Niskin-type bottles (18.5 L) with standard sampling spigots for gas collection and Teflon stopcocks for trace metal and trace particulate sample collection. The bottles were closed using Silastic springs and the endcaps were fitted with Viton O-rings. The CTD cable was a standard steel cable. No special effort was made to clean the Niskin bottles. Hydrocasts were conducted as vertical casts with a single round trip between the ship and the depth of interest and as towed hydrocasts in which the CTD-rosette package was raised and lowered as the ship moved along a set course. Light scattering anomalies (ΔNTU) are the difference between the light scatter value measured in a plume and that of the local background in nephelometric turbidity units (NTU). The ORP sensor measures the potential between a platinum electrode and a silver-silver chloride reference electrode. Laboratory experiments demonstrate that this sensor responds to Fe^{2+} and sulfide at nanomolar levels. Oxygen levels in seawater (80–200 μM) compared to the relatively small amounts of H_2S and Fe^{2+} (0.1–10 μM) in the plumes indicate that this sensor does not measure the actual "oxidation reduction potential" of the seawater but instead must respond to reduced species oxidizing at the surface of the Pt electrode, thereby producing a potential relative to the reference electrode. Here we call the change in this potential versus that of background seawater ΔE.

[6] Samples for total dissolvable Mn and Fe (TDMn and TDFe) were collected directly from the Teflon stopcocks into 125 mL I-Chem polyethylene bottles, while dissolved Mn and Fe (DMn and DFe) samples were collected as the filtrate from 0.4 μM acid-washed polycarbonate filters into 125 mL I-Chem polyethylene bottles after the passage of 2 L of water through the filters. The metals samples were then acidified with 0.5 mL of subboiling quartz distilled 6N HCl. Mn was determined with a precision of 1 nM by modifying the direct injection method of *Resing and Mottl* [1992] by adding 4 g of nitrilo-triacetic acid to each liter of buffer. Fe was determined with a precision of ±2 nM by modifying the method of *Measures et al.* [1995] for direct injection analysis. Total CO_2 (ΣCO_2) was sampled and determined by standard methods [*U. S. Department of Energy*, 1994]. The pH samples were collected and analyzed as discussed previously [*Resing et al.*, 2004]. Changes in pH (ΔpH) and ΣCO_2 (ΔCO_2) were calculated by subtracting the regional background value of each. Hydrogen sulfide (H_2S) was determined on samples following the procedure of *Sakamoto-Arnold et al.* [1986].

[7] Elemental composition of particulate matter was determined by X-ray primary- and secondary-emission spectrometry with a Pd source and Mo, Ti, Ge, and Co secondary targets using a nondestructive thin-film technique [*Feely et al.*, 1991]. Precision averaged 2% for major elements, 7% for trace elements, and 11% for sulfur. Particulate compositions are designated by a "p" in front of the element of interest (e.g., particulate Al = pAl). Total particulate Sulfur (pS) is a combination of elemental sulfur (pS_{El}) and nonvolatile sulfides + sulfates (S_{NV}). It is analyzed under an atmosphere of nitrogen. Elemental sulfur sublimes under a vacuum leaving pS_{NV}, thus pS_{El} is the difference between total pS and the sulfur concentration determined under a vacuum. He concentrations and isotopic ratios were determined on samples sealed into copper tubing [*Young and Lupton*, 1983] followed by analysis on a 21-cm radius, dual-collector mass spectrometer with a precision of $\pm 2 \times 10^{-17}$ mol kg^{-1} in ^{3}He and ±0.2% in $^3\delta$He. Samples for methane concentration were drawn into 140 ml syringes and analyzed on board via a helium head

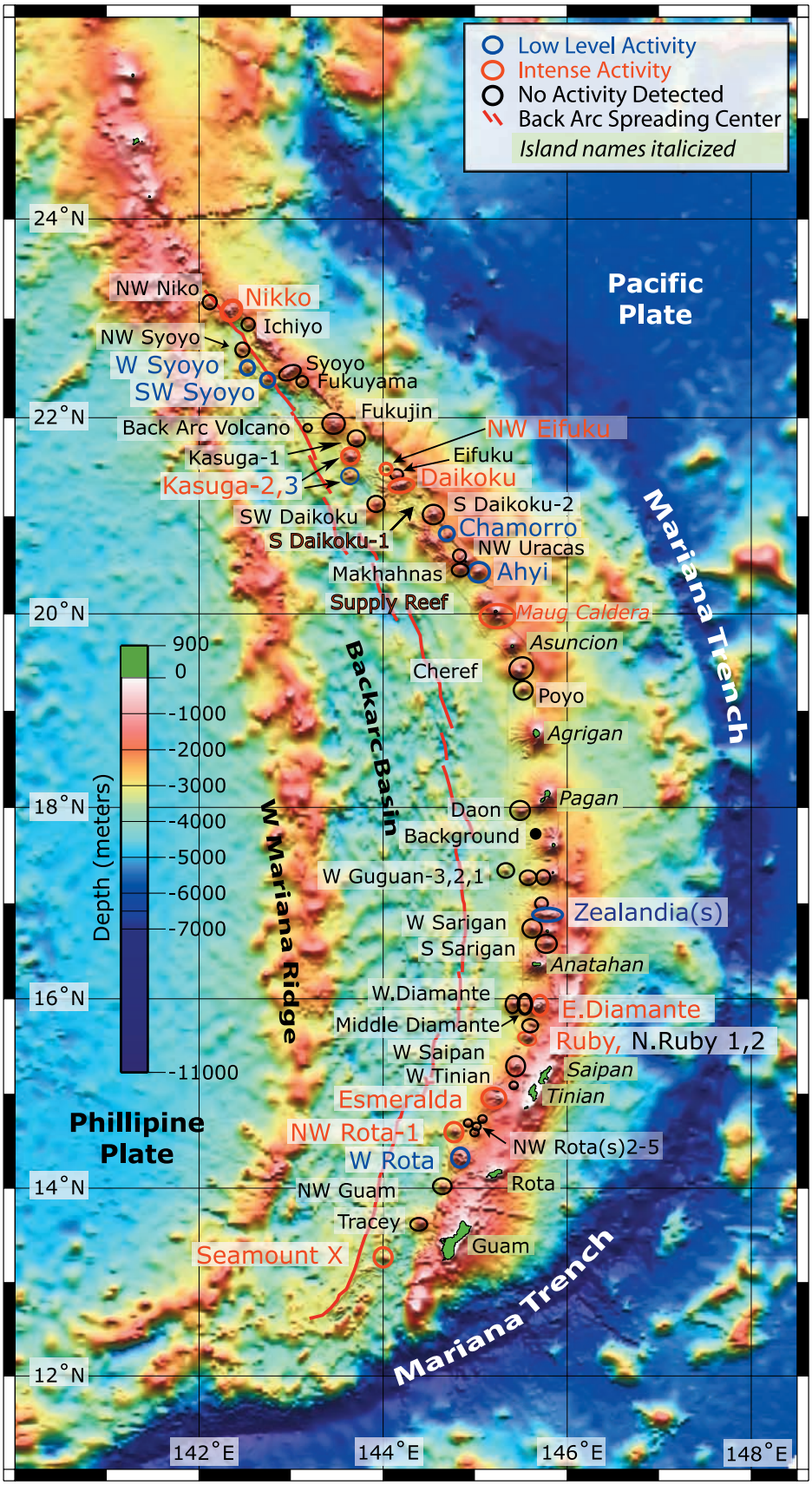
Low Level Activity
Intense Activity
No Activity Detected
Back Arc Spreading Center
Island names italicized
24°N
22°N
20°N
18°N
16°N
14°N
12°N
142°E
144°E
146°E
148°E
Pacific Plate
Phillipine Plate
Mariana Trench
Mariana Trench
Backarc Basin
W Mariana Ridge
Depth (meters)
900
0
-1000
-2000
-3000
-4000
-5000
-6000
-7000
-11000
NW Niko
Nikko
Ichiyo
NW Syoyo
W Syoyo
SW Syoyo
Syoyo
Fukuyama
Fukujin
Back Arc Volcano
Kasuga-1
Kasuga-2,3
NW Eifuku
Eifuku
Daikoku
SW Daikoku
S Daikoku-1
S Daikoku-2
Chamorro
NW Uracas
Ahyi
Makhahnas
Supply Reef
Maug Caldera
Asuncion
Cheref
Poyo
Agrigan
Pagan
Daon
Background
W Guguan-3,2,1
Zealandia(s)
W Sarigan
S Sarigan
Anatahan
W.Diamante
E.Diamante
Middle Diamante
Ruby, N.Ruby 1,2
W Saipan
W Tinian
Saipan
Tinian
Esmeralda
NW Rota-1
NW Rota(s)2-5
W Rota
Rota
NW Guam
Tracey
Guam
Seamount X

Figure 1

space technique by gas chromatography within hours of sampling [e.g., *Kelley et al.*, 1998].

[8] The parameters of the carbonate system (pCO_2, pH, alkalinity, and ΣCO_2) are thermodynamically related and only two of the parameters are required to fully describe the carbonate system [*Millero*, 1979]. These relationships have been incorporated into a computer program [*Lewis and Wallace*, 1998] that requires the input of salinity, temperature, depth, silica, phosphate, and two of the carbon system parameters to yield the remaining system parameters. The starting conditions (depth, silica, phosphate, ΣCO_2, and alkalinity) for each volcano were determined from the data collected on WOCE section P-10 at equivalent latitudes and depths [*Sabine et al.*, 1999]. This program was used to model the additions of different hydrothermal fluids to ambient seawater.

4. Results

[9] Of the 50 submarine volcanoes surveyed on the Mariana Arc during this study (Figure 1, auxiliary material), we found clear evidence for hydrothermal activity on 16 of them (Figure 2 and Tables 1, 2, 3, and 4; auxiliary material), while another two exhibited very limited evidence of activity (Table 4). We failed to find hydrothermal activity at several other volcanoes that had historical records of eruptive activity. In examining the volcanoes, we divide them into those with strong, weak, and no hydrothermal activity. We define strong activity as hydrothermal plumes with chemical anomalies that are large enough to enable us to make an evaluation of the source fluids and the hydrothermal setting from which they arose. Weak activity is defined by volcanoes having much smaller chemical anomalies (Figure 3; Table 4) which do not allow for source fluid characterization. In general, $\Delta^3He = 0.5$ fM is the threshold separating strong and weak activity. The exception to this is E. Diamante, which had an intense particle plume [*Baker et al.*, 2008] but a Δ^3He 0.2 fM.

4.1. Strong Hydrothermal Activity

[10] *Seamount X* exhibited moderate ΔNTU and weak ΔE signals over the depth range of 1200 to 1350 m during a towed hydrocast (T03A03) offset 150 m SE from the summit (Figure 2). Samples collected showed significant increases in TDFe, TDMn, and ^3He with a smaller increase in pS (nonvolatile plus volatile sulfur) (Tables 2 and 3 and auxiliary material). Both Fe (73–93%) and Mn (100%) were mostly in the dissolved phase, indicating that the samples collected were of freshly vented fluids. On the whole, the correlation between TDFe and TDMn was poor. When the data were subdivided into shallower and deeper samples, however, the correlation improved with the shallower samples having an Fe:Mn = 1.2:1 and the deeper ones a ratio of 4:1. The highest concentrations of pS were also in the shallow samples, while the deeper ones had very little sulfur. Elemental sulfur most likely arises from the oxidation of H_2S [*Resing et al.*, 2004] and its presence indicates a hydrothermal source where H_2S > Fe. This would produce low Fe:Mn in the shallower samples due to the formation of Fe sulfides. Samples were not collected for ΣCO_2; however, an upper limit for the amount of excess CO_2 added to the plumes can be made by assuming that the pH anomaly was caused solely by CO_2 [see *Resing et al.*, 2004]. The pH decrease of 0.1 pH unit suggests, therefore, that the largest possible ΔCO_2 34 μM and an upper limit for ΔCO_2:^3He is 28×10^9.

4.1.1. NW Rota-1

[11] Hydrothermal activity was identified during a towed hydrocast (T03A06) northwest of the summit by large ΔNTU signals 460-m depth, 60 m above the summit of the volcano, with a secondary plume at 520-m depth. The plume samples showed extremely elevated TDFe, TDMn, pAl, pS, CO_2, ^3He, and ΔpH (Figure 2; Tables 2 and 3; auxiliary material). These plumes, described previously [*Resing et al.*, 2007], have an abundance of alunite crystals, weathered and reprecipitated silicas, and clays. In repeat visits to this volcano in 2004, 2005, and 2006, it was found to be in a continuous state of eruption [*Chadwick et al.*, 2008; *Embley et al.*, 2006] producing large clouds of volcanic ash and glass [*Walker et al.*, 2008]. Over this time period, the volcano was found to be venting highly acidic fluids rich in sulfurous acid (D. A. Butterfield, personal communication, 2008), greatly increasing ΔpH observed in the plume (Figure 4).

Figure 1. Regional map of the Mariana Arc. Circles denote volcanoes that were surveyed during this study. Red circles and red labels indicate submarine volcanoes with moderate to intense activity. Blue circles and labels indicate volcanoes with low-level activity. Black circles indicate that no activity was identified during this survey. South Daikoku and Supply Reef were not surveyed.

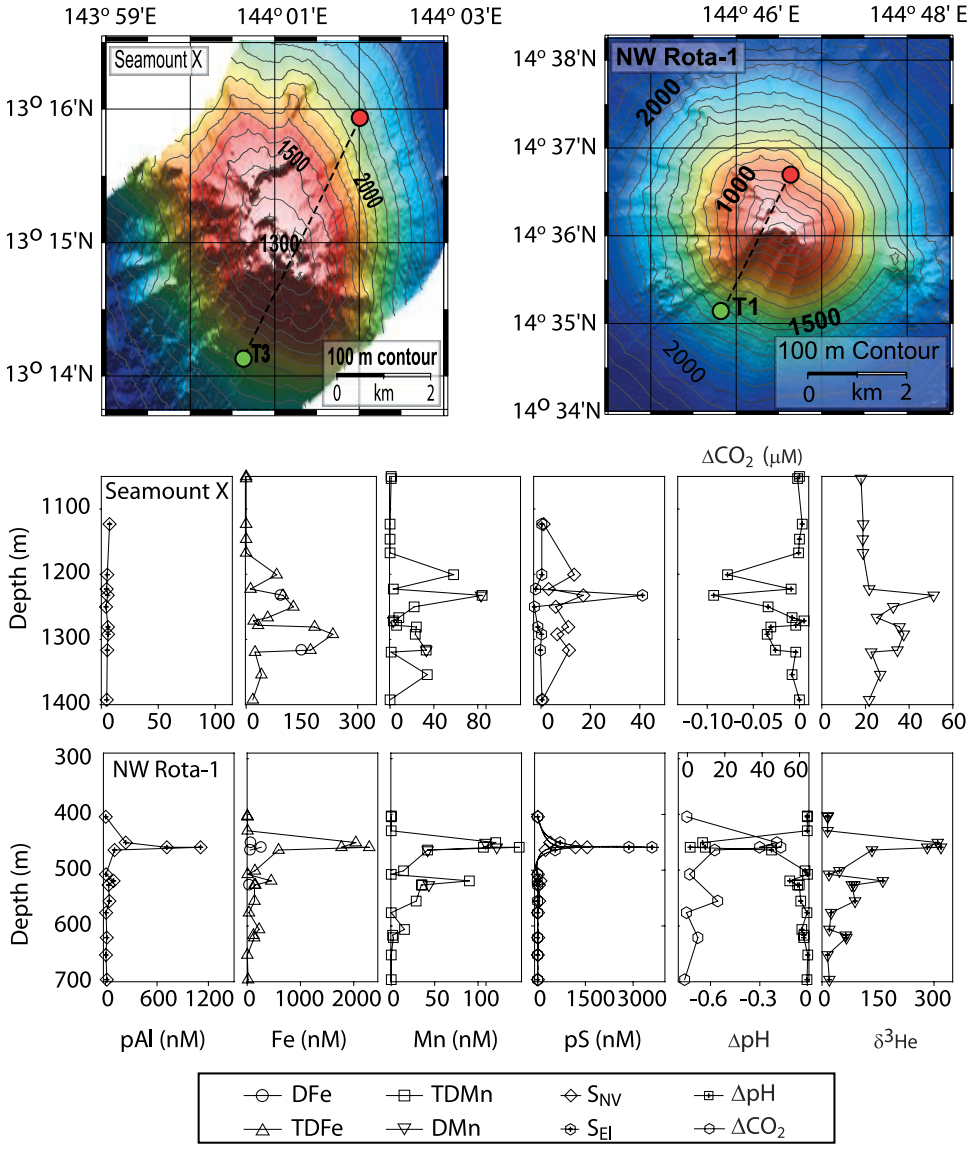

Figure 2. Bathymetric maps of hydrothermally active volcanoes and vertical profiles of chemical anomalies above them. Tows are indicated by black lines on the maps with green and red circles indicating the starting and ending points of the tows, respectively. Locations of vertical casts are indicated by yellow filled symbols. Note that scales are different for each volcano. Particulate aluminum and sulfur are designated by pAl and pS, respectively. Here pS equals elemental sulfur (pS_{El}) plus nonvolatile sulfur (pS_{NV}). Total dissolvable Fe and Mn (TDFe and TDMn) are the total amount of Fe and Mn in unfiltered acidified samples, while dissolved Fe and Mn (DFe and DMn) are the amount of Fe and Mn in filtered acidified samples. Here ΔpH and ΔCO_2 are the changes in pH and CO_2 from the regional background, respectively.

4.1.2. Esmeralda Bank

[12] Esmeralda Bank was surveyed using vertical hydrocasts (Figure 2) into the caldera (V03–07) and on a cone on the northern caldera wall (V03–08) where hydrothermal activity had been previously identified [*Stüben et al.*, 1992]. Hydrothermal activity was identified within the caldera from a large ΔNTU signal below the 225-m sill depth and by elevated levels of TDFe, TDMn, CO_2, ^{3}He, CH_4, and ΔpH (Figure 2; Tables 2, 3; auxiliary material). Fe was found entirely in the particulate phase while Mn was 100% dissolved. The lack of dissolved Fe suggests that the fluids that we sampled in the caldera were hours to several days old [e.g., *Massoth et al.*, 1998], but the fact that the Mn was 100% in the dissolved phase suggests that the fluids that we sampled were younger than a few weeks [*Cowen et al.*, 1990; *Kadko et al.*, 1990].

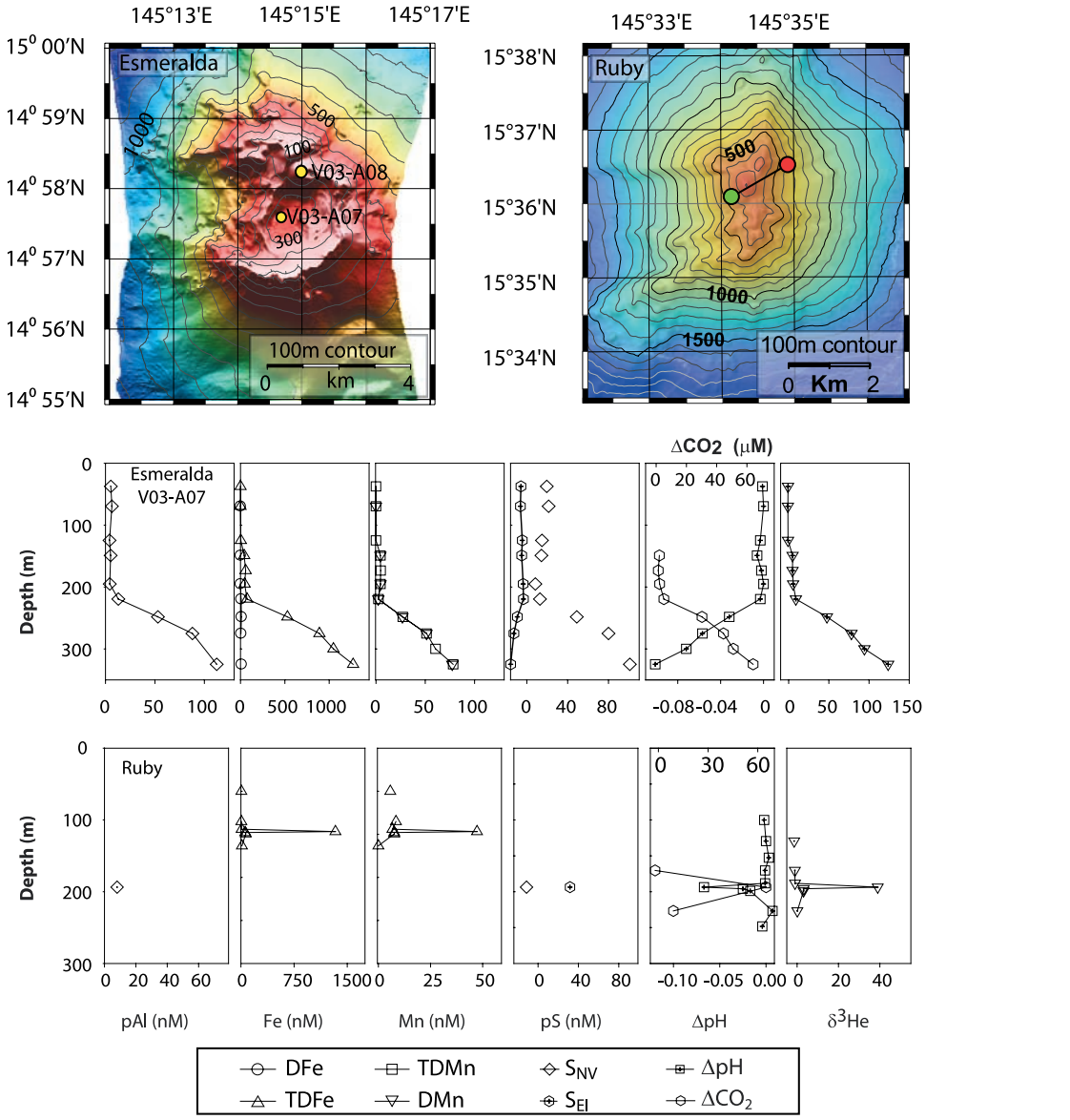

Figure 2. (continued)

TDFe and TDMn were well correlated (R^2 = 1.00) with a slope of 17:1, Fe:Mn. The increases in CO_2 correlated well with increases in ^{3}He (R^2 = 0.97) and decreases in ΔpH (R^2 = 0.98). No H_2S was detected in samples from Esmeralda. The trend in ΔpH versus ΔCO_2 indicates the venting of CO_2- and alkalinity-rich fluids.

4.1.3. Ruby

[13] A towed hydrocast (T03A-08) to the east of the summit in 2003 revealed no hydrothermal activity. Because eruptive activity had been reported as recently as 1995 [*Venzke et al.*, 2002], a second towed hydrocast (T06A-07) was made to the S-SE of the summit in 2006. Hydrothermal activity was indicated by moderate ΔNTU and ΔE signals. Follow-up chemical analyses revealed significant increases in TDFe, TDMn, pFe, CO_2, ^{3}He, and ΔpH (Tables 2 and 3; Figure 2; auxiliary material). The trend in ΔpH versus ΔCO_2 indicate venting of CO_2- and alkalinity- rich fluids.

4.1.4. East Diamante

[14] Hydrothermal activity was identified during a towed hydrocast (T03A-09) by a large ΔNTU signal in the caldera. Analysis of the particulate matter reveals that the ΔNTU signal was caused by pS_{El} (up to 700 nM) with little to no pFe. TDFe and TDMn were also low, reaching only ~12 nM and 3.4 nM, respectively (Figure 2). A moderate ΔpH

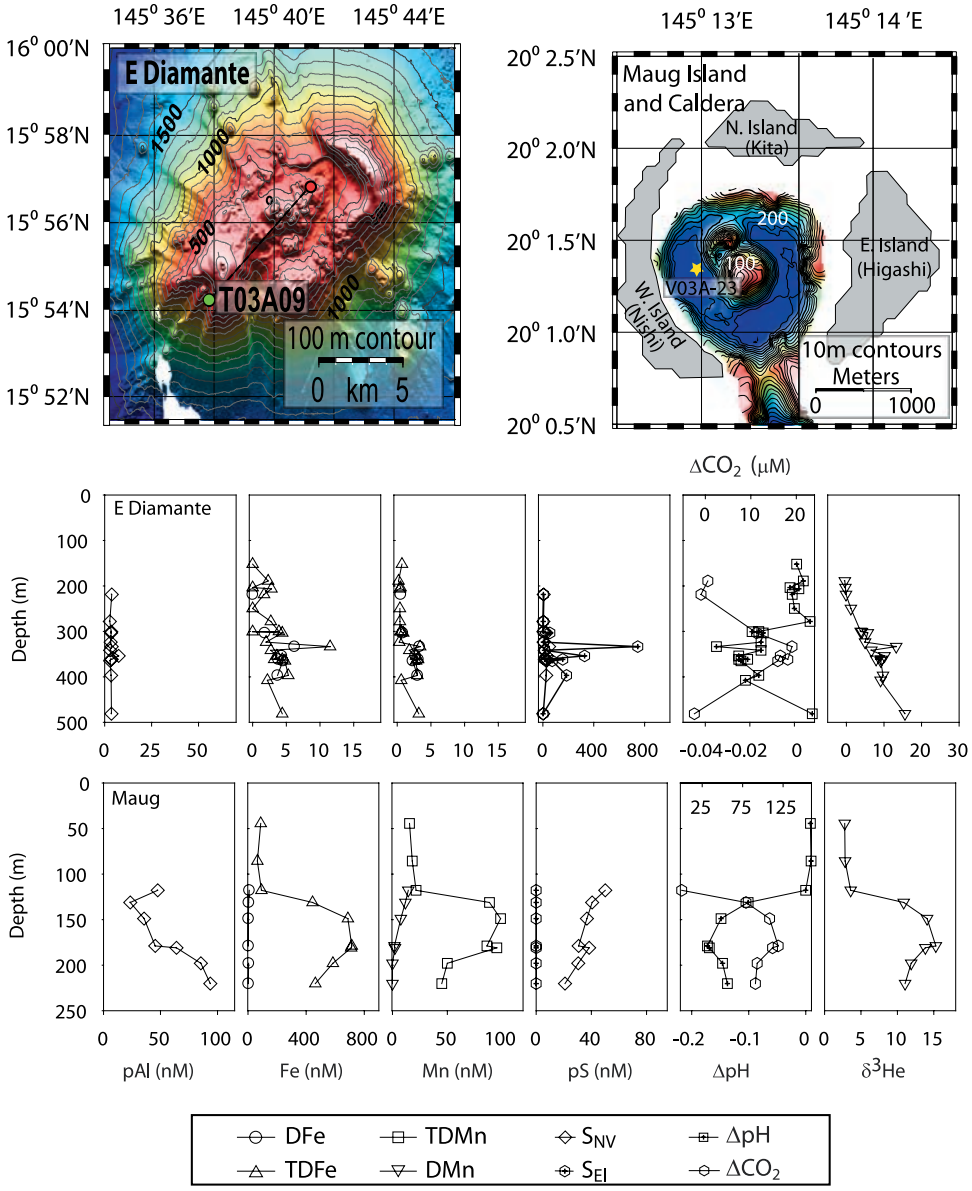

Figure 2. (continued)

of −0.035 pH units and a very weak ^{3}He = 0.2 fM was also present. Although ΔpH and ΔCO_2 were relatively small, their relationship indicates the venting of CO_2- and alkalinity-rich fluids.

[15] The chemistry of the observed plume is inconsistent with the black smokers found at this site when visited by a ROV in 2004 [*Embley et al.*, 2007]. High-temperature venting should produce plumes richer in Mn and ^{3}He than the values observed here. Clearly, the black smokers contribute little to the hydrothermal plumes observed here and the plume was formed from some other source very rich in sulfur. This will be discussed further below.

4.1.5. Maug

[16] Maug was surveyed using a single vertical cast (V03A-23) into a basin formed by a central cone and the western walls of the caldera. ΔNTU signals normally associated with the shallow ocean, combined with the enclosed caldera, made evaluation of the hydrothermal plume from ΔNTU problematic. As a result, samples were collected at fixed depths and evaluations of activity relied on postcruise chemical analysis. These analyses revealed a large enrichment in ^{3}He in the caldera with relatively elevated ^{3}He reaching the shallowest sample at 44-m depth (Figure 2). Unlike other samples collected in the near surface ocean, the

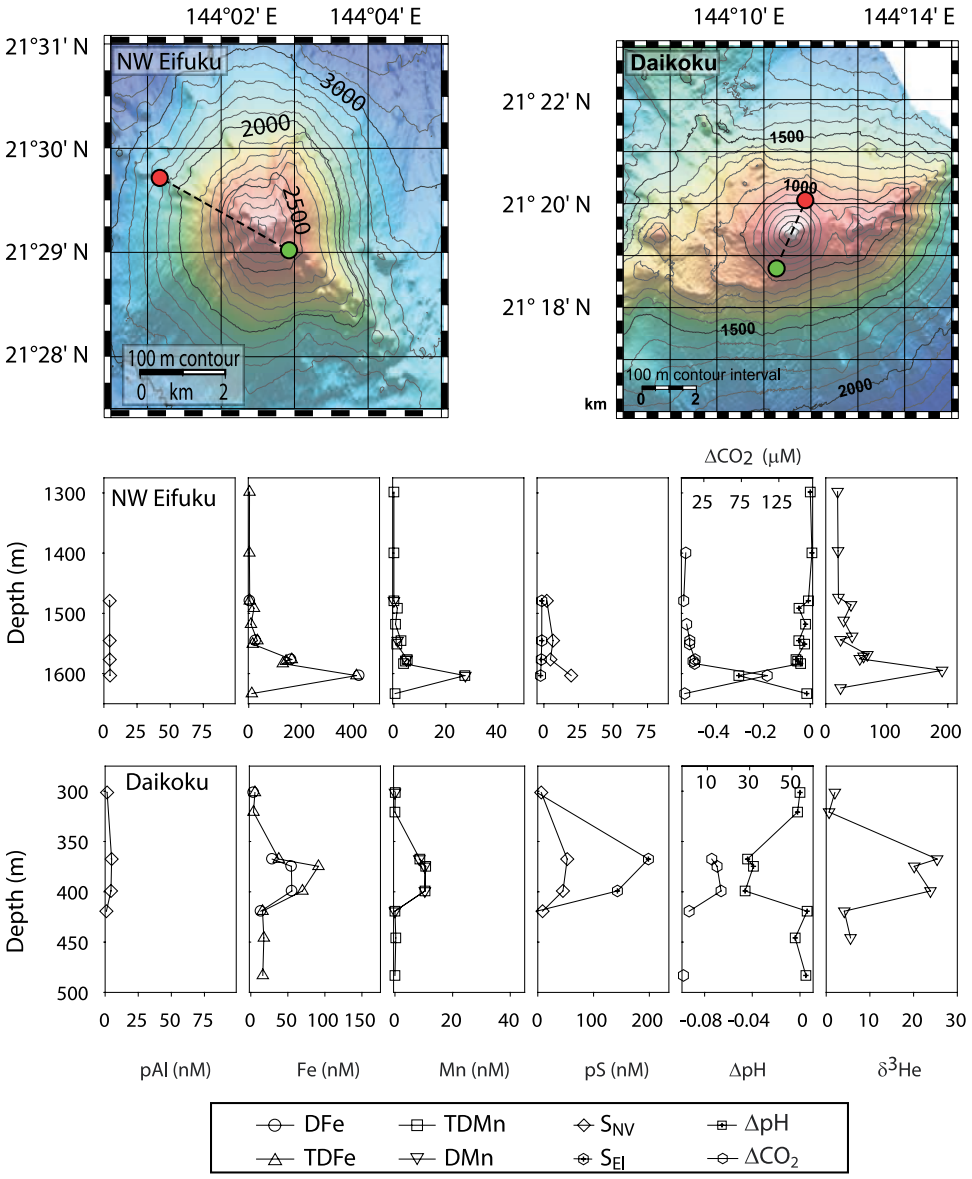

Figure 2. (continued)

δ^3He in the sample at 44 m does not drop below 0% but is enriched, indicating that the waters in the caldera are actively degassing to the atmosphere. Other strong chemical enrichments were observed in ΣCO_2, TDMn, TDFe, pFe, pMn, and ΔpH. In this instance, both Fe and Mn were completely in the particulate phase. In fact, the concentration of pMn (determined on the filters) exceeded that of total acid soluble Mn (TDMn), indicating that the acid added to the whole water sample was unable to dissolve all of the pMn. The relationship between ΔpH and ΔCO_2 indicate the venting of CO_2- and alkalinity-rich fluids.

4.1.6. Daikoku

[17] Daikoku was surveyed using a towed hydrocast (T03A-32) to the SSE of the summit. A hydrothermal plume detected from both ΔNTU and ΔE was found below the summit at 375 m depth, suggesting that the source of the fluids must lie along the flanks of the volcano. This is consistent with ROV visits to the area that discovered a 50-m-wide crater on the north flank of the volcano, 75 m below the summit, that was actively venting cloudy white hydrothermal effluent. The plume coming from Daikoku was moderately enriched in TDFe, TDMn, CO_2, ^{3}He, and ΔpH (Figure 2). A much larger anomaly for H_2S and pS was observed

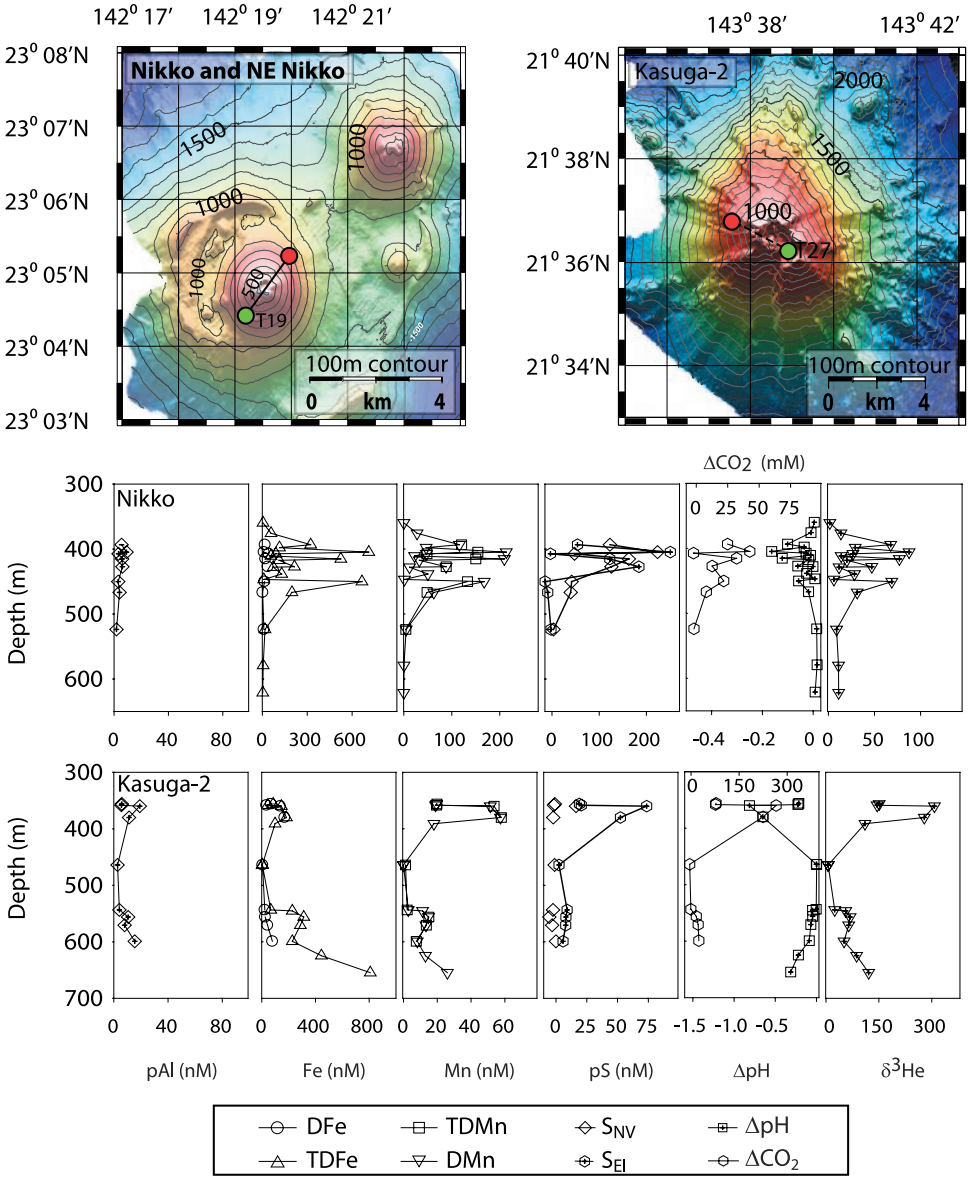

Figure 2. (continued)

and this pS was predominantly pS_{EI}, which is consistent with the cloudy white fluids being emitted from the flank crater. The presence of H_2S and 70% of the Fe in the dissolved phase suggest a low oxygen setting and/or that the fluids were collected very near the source. ΔpH and ΔCO_2 were very small and their relationship exhibited scatter; however, the data suggest that the plume was influenced by both CO_2 and H^+.

4.1.7. NW Eifuku

[18] Hydrothermal activity was identified during a towed hydrocast (T03A30) over the volcano summit by a large ΔE signal. The plume was enriched in TDFe, TDMn, ^3He, H_2S, CO_2, and ΔpH (Tables 2, 3; Figure 2; auxiliary material). The very small ΔNTU in the plume is inconsistent with the elevated levels of pFe found. The relationship between ΔpH and ΔCO_2 indicates that pH changes were brought about solely by ΔCO_2.

4.1.8. Kasuga-2

[19] Kasuga-2 was surveyed using a towed hydrocast (T03-A27) that started within the caldera, proceeding northwest of the summit and down the flank. Two separate hydrothermal sources were identified during the hydrocast: a deep plume at 550-m to 650-m depth and a shallow plume at 355-

Table 1. Hydrothermally Active Submarine Volcanoes of Mariana Arc Sampled During This Study

	Summit Depth (m)	Caldera Floor Depth (m)	Plume Depth (m)	Morphology	Rock Type	Chemical Characteristics of Venting
Seamount X	1230	-	1250,1290	Cone	B/BA[a]	Moderate Fe, Mn and ^{3}He
NW Rota-1	520	-	450	Cone	B-BA-A[b]	Acid Rich, Fe, Al, S,
West Rota	400	1400	1160	Caldera	B-A-D[c]	Small Fe, Mn, and ^{3}He
Esmeralda Bank	<100	300	>220	Caldera	B/BA[d]	CO_2 and Alkalinity, Fe
Ruby	175	-	200	Cone	Basalt[e]	CO_2 and Alkalinity, Fe
E Diamante	125	500	300	Caldera	Dacite[f]	Sulfur and Gas, no Metals
W Diamante[g]	400	-	550	Eroded Cone	B/BA[h]	Very Small ^{3}He anomaly
Zealandia	500	?	600	Caldera?	B/A[i]	Small Fe, Mn, and ^{3}He
Maug	Surface	250	>150	Cone in Caldera	Basalt[j]	CO_2 and Alkalinity, Fe
Ahyi	<100	-	90	Cone	Basalt[k]	Small ^{3}He anomaly
NW Uracas[g]	750	>900	922	Caldera	Basalt[k]	Very Small ^{3}He anomaly
Chamorro	825	-	875	Eroded Cone	Dacite[k]	Small ^{3}He anomaly
Daikoku	325	-	375	Cone	Andesite[k]	CO_2 Rich, Low T, S-oxidation
Kasuga 2	400	650	380,650	Caldera	B/BA[l]	CO_2 Rich, High T
SW Soyo	1450	-	1675	Caldera	-	Small Mn and ^{3}He
W Soyo	1750	2150	2050	Caldera	-	Small Mn and ^{3}He
NW Eifuku	1600	-	1600	Cone	Basalt[m]	CO_2 Rich, Low T
Nikko	400	-	400,450	Caldera	B/D[n]	CO_2, High T, S-oxid. Sulfide

[a] Basalt and basaltic andesite [*Fryer et al.*, 1998].
[b] Basalt, basaltic andesite and andesite [*Stern et al.*, 2008].
[c] Basalt, andesite, and dacite [*Stern et al.*, 2008].
[d] Basaltic and basaltic andesite [*Stern and Bibee*, 1984].
[e] *Stern et al.* [1989].
[f] Composition of resurgent dacite dome [*Stern et al.*, 2004].
[g] Evidence of activity at W Diamante and NW Uracas is not definitive and these volcanoes should not be considered active without more conclusive evidence.
[h] Basaltic and basaltic andesite [*Dixon et al.*, 1984].
[i] Basalt and andesite [*Dixon et al.*, 1984].
[j] *Woodhead* [1989].
[k] *Bloomer et al.* [1989].
[l] Basalt and andesite [*Fryer et al.*, 1997].
[m] *Stern et al.* [2004].
[n] Basalt and dacite [*Bloomer et al.*, 1989].

Table 2. Maximum Concentrations of Dissolved and Particulate Components in Hydrothermal Plumes Above Hydrothermally Active Submarine Volcanoes[a]

	ΔNTU	ΔE (mV)	pFe	TDFe (nM)	% DFe	TDMn (nM)	% DMn	Fe:Mn	pS_{EL} (nM)	pS_{NV} (nM)	pAl (nM)	pSi (nM)
Seamount X												
Shallow	0.018	−78	6	99	93%	84	100%	1	41	17	7	2
Deep	0.022	−87	48	230	72%	34	100%	7	0	11	6	30
NW Rota	∼4.9	−490	2052	2300	<10%	150	>95%	14	3594	1560	1100	650
Esmeralda Bank	0.4	nd	1048	1270	<1%	78	>95%	17	0	100	112	270
Ruby	0.044	−23	1568	1333	85%	47	>98%	26	0	30	8	44
E Diamante	0.62	−38	2.2	11.5	50%	3.2	95%	1.5	700	50	4	18
Maug	0.26	nd	1238	700	<1%	98	0–75	7	0	50	95	330
Daikoku	0.095	−104	22	91	70%	11	>98%	5	200	53	5	32
NW Eifuku	0.012	−119	4	400	100%	27	100%	15	17	19	4	22
Kasuga −2												
Shallow	0.485	−290	24	180	86%	58	>98%	2.8	16	74	20	50
Deep	0.06	∼−70	263[b]	810	35%	26	>98%	30	0	9	11	50
Nikko	0.222	−155	502	711	4%	214	100%	3.1	251	223	10	42
Background			1–4	2		∼0.2			2–4	2–4	1–10	10–30

[a] Ratios are derived from regressions of all samples collected. TDMn is total dissolvable Mn; DMn is dissolved Mn; TDFe is total dissolvable Fe; DFe is dissolved Fe; pAl is particulate aluminum; pSi is particulate silica; pS is particulate elemental sulfur; pS_{NV} is the sum of sulfate and sulfide sulfur which are nonvolatile (NV); na is not analyzed; ns is not sampled; and nd is not detected.
[b] Particulate Fe is from a different sample than all other chemical data listed for deep plume; see auxiliary material.

Table 3. Geochemistry of Dissolved Gasses in Hydrothermal Plumes Above Hydrothermally Active Submarine Volcanoes[a]

	CH_4 (nM)	H_2S (uM)	δ^3He[b] (%)	Δ^3He[c] fM	ΔpH	ΔCO_2	R/R_A	CO_2:^3He X10^9	% C from slab	^3He:Mn X10^{-9}	ΔCO_2: ΔpH	CO_2/H^+ %	% alkalinity
Seamount X													
Shallow	4.9	ns	51	1	−0.093	ns	7.3 ± 0.4	32 ± 1[d]	94%	12 ± 0.2	-	-	-
Deep	1.6	ns	38	0.5	−0.035	ns	5.4 ± 0.6	24 ± 3[d]	92%	12 ± 5	-	-	-
NW Rota	5	nd	314	15.3	−0.730	40	8.4 ± 0.1	3.2 ± 0.2	38%	109 ± 5	65 ± 5	20/80	-
Esmeralda	20	nd	120	4.3	−0.100	64	6.7 ± 0.6	15 ± 1	87%	55 ± 2	657 ± 41	-	20%
Ruby	ns	ns	39	1.1	−0.067	65	7.6 ± 0.6	54 ± 6	96%	26 ± 3	856 ± 223	-	40%
E. Diamante	2.5	nd	8	0.2	−0.035	19	nr	nr		nr	561 ± 50		30%
Maug	90	nd	249	12.8	−0.170	119	7.0 ± 0.2[e]	10 ± 1	80%	130 ± 24	668 ± 44	-	25%
Daikoku	2.5	1.1	23	0.7	−0.050	16	nr	nr		58 ± 7	326 ± 54	nr[f]	-
NW Eifuku	4.7	1.0	170	7.3	−0.305	110	7.2 ± 0.1	15 ± 1	87%	270 ± 6	368 ± 17	100/0	-
Kasuga 2													
Shallow	94	13.9	306	15.5	−0.813	265	8.0 ± 0.5	18 ± 1	89%	259 ± 43	333 ± 12	87/13	
Deep	22	nd	108	3.8	−0.313	24[g]	7.5 ± 0.2	14 ± 4	86%	155 ± 14	333 ± 31	100/0	
Nikko	4.5	1.9	84	2.8	−0.160	43	6.6 ± 0.3	17 ± 2	88%	12 ± 1	261 ± 34	65/35	
Background	0.5–2	0			-		-	-			-		

[a] Ratios are derived from regressions of all samples collected; ns is not sampled; nd is not detected; BD is below limit of determination; and nr is not resolvable. The relative CO_2/H^+ and % alkalinity were calculated by modeling relationship between CO_2 and pH upon addition of different fluids to ambient seawater (see Figure 4).
[b] Above background.
[c] ^3He above background.
[d] Calculated by assuming all pH change from CO_2.
[e] Eliminated data point V23–4, with all data $R/R_a = 6.6 \pm 0.3$.
[f] Data fit suggest 75/25 with considerable scatter.
[g] Total CO_2 is from a different sample than all other data, see auxiliary material.

to 390-m depth (Figure 2). The shallow plume exhibited the greater ΔNTU and ΔE signals. The shallower plume was located near but below the summit, 20–35 m above the local bottom, suggesting a shoulder on the western peak as the source of the fluids. Each of the two sources has a distinct chemistry. ΔCO_2 and δ^3He were the first and second largest observed during this survey, respectively. The shallow plume was also enriched in TDFe and TDMn, with an Fe:Mn of 2.8. The Fe was mostly (86%) in the dissolved phase. This elevated DFe and the presence of H_2S in the plume suggest that we sampled recently vented fluids. The ΔNTU is very high in the summit plume

Table 4. Low Levels of Activity[a]

	PFe	TDFe (nM)	TDMn (nM)	δ^3He	δ^3He Background[b]	^3He (fM)	^3He (fM) Background[b]	Δ^3He (fM)	ΔpH
Clear Evidence of Hydrothermal Activity									
Zealandia	ns	16	10	20.8	11	3.09	2.89	0.3	nr
West Rota	ns	12	12	22.7	18	3.21	3.09	0.12	0.006
Chamorro	ns	na	na	19.8	15.5	3.1	2.94	0.16	nr
SW Syoyo	ns	na	5	28.5	19	3.41	3.14	0.27	0.004
W Syoyo	3.6	na	0.9	24.4	20	3.29	3.15	0.14	nr
Ahyi	na	na	na	2.5	−1.2	2.43	2.36	0.07	nr
Some Evidence for Hydrothermal Activity									
W Diamante	ns	na	0.7	14.9	14.1	2.9	2.85	0.05	nr
NW Uracas	10	5	na	15.6	14.9	2.93	2.91	0.02	
Background	1–4	2	0.2						

[a] Maximum concentrations of dissolved and particulate components in hydrothermal plumes above active submarine volcanoes; pFe is particulate Fe; ns is not sampled; TDMn is total dissolvable Mn; na is not analyzed; TDFe is total dissolvable Fe; nr is not resolvable; $\Delta^3He = {}^3He_{sample} - {}^3He_{background}$.
[b] Local background.

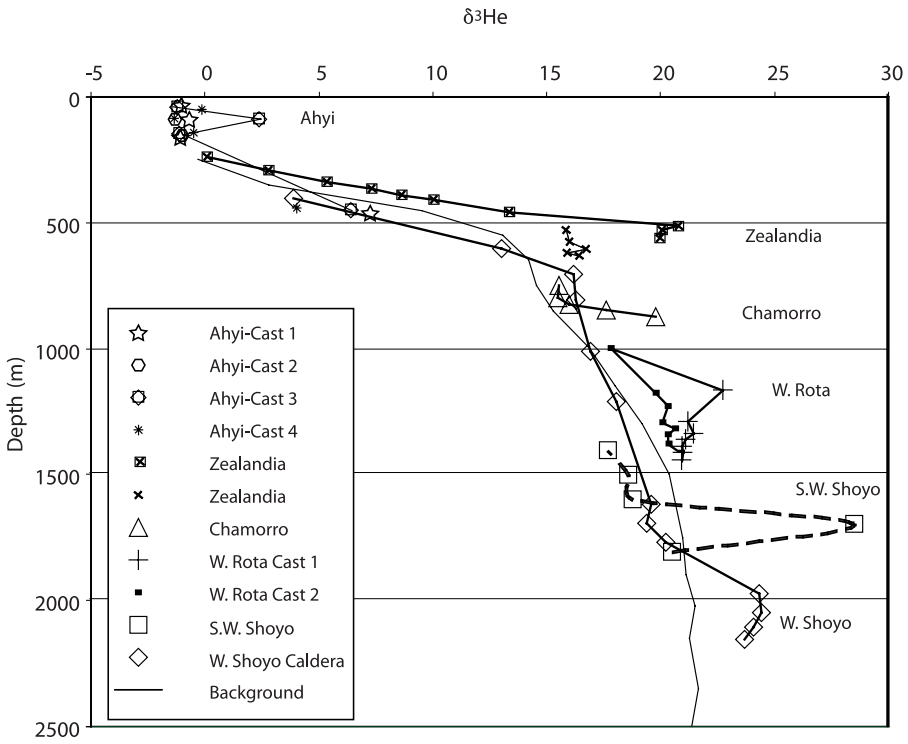

Figure 3. Low-level venting as identified by helium isotopic data. The solid line represents the background of the δ^3He along the arc; however, it is based on a single location at ~18°N in the study area (see Figure 1). Although this background is not fully representative of the background at different particular sites within the study area, its overall shape is. During individual casts, the δ^3He levels above and below the plumes are more representative of local background. Of the four casts taken around the summit of Ahyi volcano, a single sample showed elevated δ^3He. The pH data indicate that this single sample was from this depth and not inadvertently collected at a deeper depth.

(0.5 NTUs) and is poorly explained by the levels of pFe and pS. We suggested previously [*Resing et al.*, 2004] that H_2S is likely oxidized to form elemental sulfur when hydrothermal fluids entrain cool oxygen-rich ambient seawater. However, it is possible that the ΔNTU might arise from polymeric sulfur species that can form prior to the large pS particles [*Luther et al.*, 2001]. These small particles may not be collected on our filters. The ratio of the change in pH to CO_2 suggests that pH changes come from both CO_2 (87%) and from H^+ (13%). However, the source of H^+ is likely from the oxidation of the H_2S in our sample bottles while the samples sat in the lab awaiting analysis

$$H_2S + O_2 = 2H^+ + SO_4^{2-}. \quad (1)$$

The oxidation of this H_2S to form H^+ would account for 11% of the pH change.

[20] The deeper plume was most intense near the caldera floor at 650 m, extending upward ~100 m. There is no sill that would retain the plume, suggesting that the hydrothermal effluent is actively rising. The deeper plume was greatly enriched in TDFe and TDMn, with TDFe being 4X higher in the deep versus the shallow plume, with 35% of the Fe in the dissolved phase. The deep plume had a much higher Fe:Mn of 30 with little pS and no H_2S. ΔCO_2 and ΔpH were smaller than in the upper plume but ΔCO_2:ΔpH fell close to the same trend line (Figure 4). The CO_2 to ^{3}He ratio was similar for both plumes, suggesting a common source for the magmatic gasses. The data suggest that the deeper source is low temperature and dominated by carbonic-acid weathering of the rocks, resulting in elevated Fe and high Fe:Mn, while the shallower source is a high-temperature gas-rich (H_2S) system resulting in lower Fe:Mn.

4.1.9. Nikko

[21] Hydrothermal activity was identified by large ΔNTU and ΔE observed during a towed hydrocast (T03A-19) over the summit. A plume depth of 465 m suggests fluids venting from the crater floor. The large ΔNTU arose from a plume rich in both pFe and pS (Figure 2). The system is metal rich,

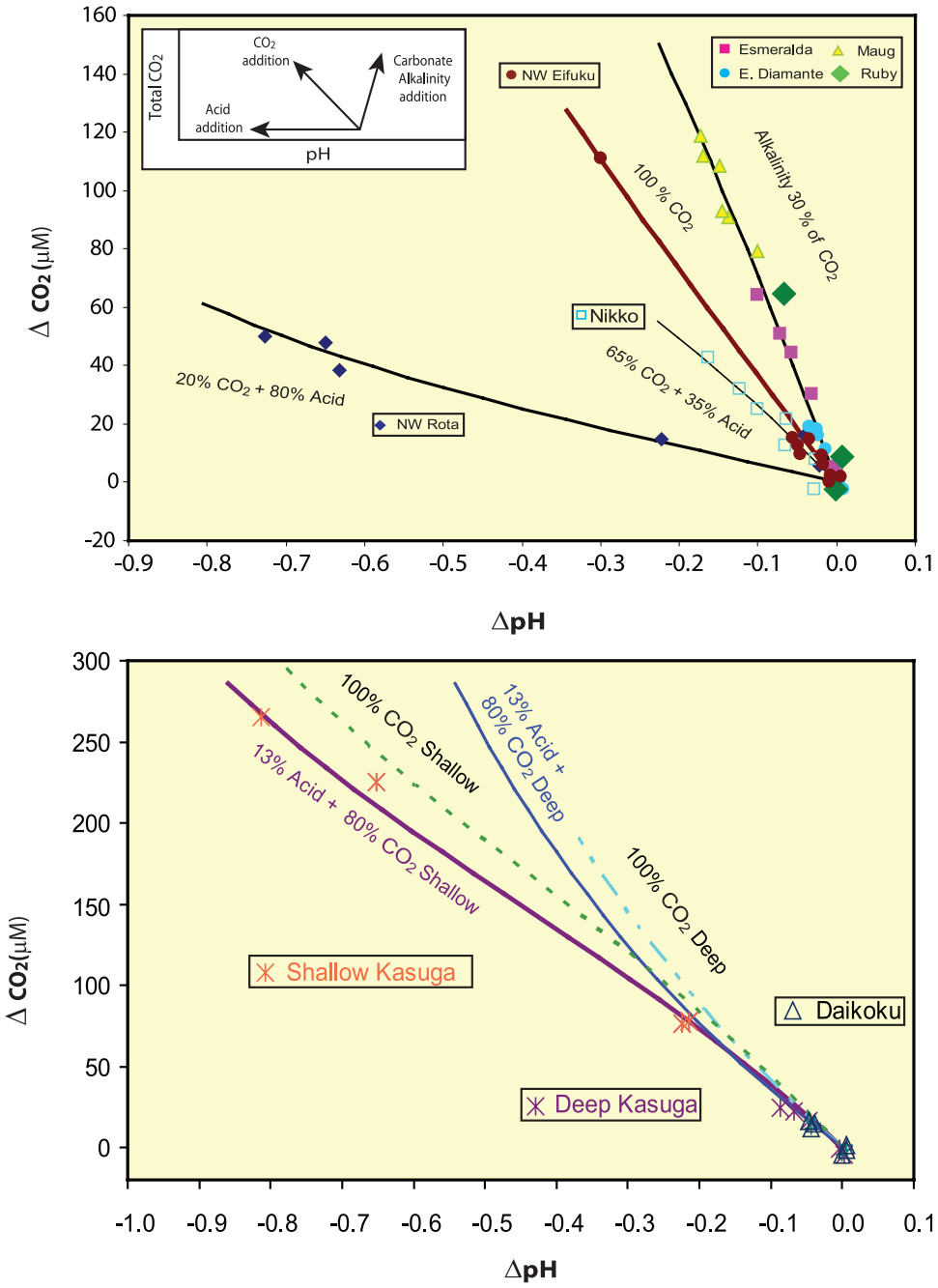

Figure 4. The values of ΔpH and ΔCO_2 are the changes in pH and ΣCO_2, respectively, from their regional backgrounds. The inset at the top shows that decreases in the pH of seawater result from the addition of CO_2 and/or mineral acidity (H^+). The addition of CO_2 decreases pH and increases ΣCO_2, while the addition of H^+ decreases pH without increasing ΣCO_2. When only CO_2 is added, the slope of ΔCO_2 versus ΔpH is approximately 360 μM/pH unit. When H^+ is added along with CO_2 the change in pH per CO_2 increases (slope decreases). When carbonate alkalinity is added pH increases; however, when both carbonate alkalinity and CO_2 are added, pH decreases, but the decrease is less than that when only CO_2 is added. The lines were generated using a seawater carbonate modeling program [*Lewis and Wallace*, 1998].

with highly elevated TDFe, and the most elevated TDMn concentrations found during this survey. Fe:Mn is 3.1:1, suggesting that these plumes may arise from high-temperature vents. The Nikko plume was also highly enriched in CO_2, ^3He, and H_2S. The particles are rich in pS_{NV} (Table 2), which likely reflects particles rich in metal-sulfides. Fe can be removed as Fe sulfides and the elevated H_2S could be responsible for the moderate to low Fe:Mn. The relatively low value of ΔCO_2: ΔpH indicates that some of the pH change arises from the addition of H^+ ions. These H^+ have several possible sources, including magmatic SO_2, H_2S oxidation, and metal sulfide formation.

4.2. Low-Level Activity

[22] The most active volcanoes were easily identified during surveys by the light scatter and ORP sensors on the CTD rosette package. However, the volcanoes with reduced activity were not easily identified by these sensors. In order to determine if these volcanoes were active, chemical analyses of Mn and ^3He were conducted on the discrete water samples collected above the volcanoes. ^3He is an unambiguous tracer of magmatic volatiles that is completely conservative, while Mn is a tracer of hydrothermal reactions that is conservative on time scales of weeks to months [*Cowen et al.*, 1990]. Examination of ^3He and available Mn data show clear evidence that six additional volcanoes were hydrothermally active: Zealandia Bank, West Rota, Chamorro, S.W. Syoyo, W. Syoyo, and Ahyi (Figure 3; Table 4; auxiliary material). Two other volcanoes, W. Diamante and NW Uracas, had barely discernable enrichments in ^3He.

4.3. No Activity

[23] We detected no activity at two volcanoes where activity was suspected based on past eruptions, Fukujin and Kasuga 3. Fukujin is one of the larger of the submarine volcanoes on the Mariana Arc whose summit is near the sea surface. Three vertical hydrocasts made near the summit showed no evidence for hydrothermal activity. The last known eruption was in 1974 and since the mid-20th century, intermittent reports of water discoloration and floating pumice have been made [*Venzke et al.*, 2002]. These results suggest that intrusive volcanism in the near surface ocean is cooled quickly, perhaps due to a more porous volcanic structure. Kasuga-3 was found to be hydrothermally active by *McMurtry et al.* [1993]. The hydrothermal activity, however, was weak and of low temperature, making it difficult to detect without a more detailed survey. There are no recorded eruptions of Kasuga-3.

5. Discussion

[24] The combination of magmatic volatiles, water-to-rock ratio, and magmatic state of the volcano contribute to the chemistry of the fluids venting from them. In particular, the amount and types of metals present (Fe, Mn, and Al) in the fluids allow us to assess the reactivity of the fluids. This reactivity is, in turn, related to the abundance of magmatic gasses (CO_2 and sulfur gasses) in these fluids, which are directly influenced by the magmatic state of the volcano. The following section characterizes the volcanoes based on these factors and places them within their magmatic-hydrothermal state.

5.1. CO_2, pH, and the Carbonate System

[25] The carbonate system within the hydrothermal plumes reflects the venting of CO_2-, acid-, and alkalinity-rich fluids from submarine volcanoes. Plume measurements show a wide array of CO_2/pH trends for the different volcanoes (Figure 4). The inset in Figure 4 demonstrates the critical relationships between pH and CO_2. Decreases in pH are brought about by the addition of CO_2 and/or mineral acidity (H^+), while the addition of alkalinity increases pH. These relationships can be modeled, allowing the assessment of where each of these volcanoes resides within the carbonate system (Tables 1 and 3) and what this reflects about an individual volcano.

[26] The simplest case is a system venting fluids that are CO_2-rich without large additions of H^+ or alkalinity. Figure 4 shows that the pH changes at NW Eifuku are caused exclusively from the addition of CO_2 (Table 3). When NW Eifuku volcano was visited using an ROV, it was found to be venting liquid CO_2 from the vent field in the presence of CO_2-clathrate [*Lupton et al.*, 2006]. The temperatures of the fluids themselves were 100°C. The presence of CO_2 without alkalinity suggests that the CO_2 did not react extensively with the host volcanic rocks to form alkalinity, because, if it had, then the change in pH with respect to CO_2 added would be less, as we will see below for other volcanoes. This finding is consistent with the presence of pure CO_2 as liquid and clathrate. In this form the CO_2 is not dissolved in water and does not react with the volcanic rocks (see discussion below).

[27] The second case is the addition of both CO_2 and H^+, which produce greater decreases in pH than just the addition of CO_2 alone. In Figure 4 we can identify four volcanoes that had pH and CO_2 changes associated with the addition of both CO_2 and H^+: NW Rota-1, Daikoku, the shallow plume at Kasuga-2, and Nikko. The amounts of H^+ and CO_2 required to produce the trends in Figure 4 can be evaluated (see methods; Table 3). These results show that the change in pH at NW-Rota-1 is dominated by the addition of acid (H^+). This results in the unique chemistry found in the plumes above the volcano [*Resing et al.*, 2007]. This volcano was found to be actively erupting when visited in 2004 and 2006 using remotely operated vehicles [*Chadwick et al.*, 2008] and the pH of the fluid exiting the volcano was <2 (D. A. Butterfield et al., manuscript in preparation, 2008). Vent and plume fluids collected in 2006 were found to be rich in sulfurous acid (B. Takano, personal communication, 2006). It is this acid that accounts for most of the change in pH observed here. Nikko and Daikoku volcanoes have plumes that are rich in elemental sulfur. ROV visits to these volcanoes identified extensive sulfur deposits and pools of liquid sulfur [*Embley et al.*, 2007]. The origin of these large S deposits is likely from magmatic SO_2:

$$3\ SO_2 + 2\ H_2O = S(0) + 2H_2SO_4. \quad (2)$$

This reaction produces both sulfur and sulfuric acid. That acid generates part of the pH change found in the plume waters. The pH changes in the shallow Kasuga-2 plume were caused mostly by CO_2 with the balance coming from the oxidation H_2S to form ^+H in the pH sampling bottles.

[28] The final case to examine is the addition of fluids rich in both CO_2 and carbonate alkalinity (HCO_3^-, CO_3^{2-}) where the change in pH in the plumes is less than that expected solely from the addition of CO_2. In gas-rich hydrothermal systems, ^+H reacts first with the host rock followed by CO_2-weathering reactions:

$$2NaAlSi_3O_8 + 2\ CO_2 + 3\ H_2O = Al_2Si_2O_5(OH)^4 + 2Na^+ + 2HCO_3^- + 4SiO_{2(aq)} \quad (3)$$

which produce alkalinity as HCO_3^-. The addition of $CO_{2(g)}$ lowers the pH of seawater while the addition of HCO_3^- increases the pH of seawater; both contribute to ΣCO_2 ($\Sigma CO_2 = CO_{2(g)} + HCO_3^- + CO_3^{2-}$). The pH changes in the plumes depend on the relative amounts of $CO_{2(g)}$ and alkalinity in the vented fluids. We observed CO_2 and HCO_3^- rich fluids at Ruby, E. Diamante, Maug, and Esmeralda where 20 to 40% of the ΣCO_2 was present as HCO_3^- (Table 3), which is much higher than the levels at Loihi Seamount where only 2–4% was present as alkalinity [*Sedwick et al.*, 1992]. The presence of alkalinity at these volcanoes is consistent with long reaction paths where H^+ is completely consumed and CO_2 reacts with the host rocks. At each of these volcanoes, except for E. Diamante, the deep-seated source of magma and CO_2 results in diffuse low temperature venting [*Embley et al.*, 2007]. E. Diamante, by contrast, had higher temperature venting and presents a unique situation that will be discussed further below.

5.2. Fe and Mn

[29] The amounts of Fe and Mn in hydrothermal plumes provide insight into the origin of the fluids being emitted from the seafloor. Although the Fe:Mn in both basalts and andesites is ~65:1 [*Govindaraju*, 1989], Fe:Mn within high-temperature hydrothermal systems are typically much lower (~1–5:1) because Fe concentrations in hydrothermal solutions are controlled by equilibrium with pyrite and other minerals, while Mn is controlled by the extraction rate of Mn from the rock and water to rock ratios [*Bowers et al.*, 1988]. The Fe levels are further reduced due to the formation of Fe sulfides upon mixing of hydrothermal fluids with cold ambient seawater. The ratio of Fe to Mn in the plumes was different from volcano to volcano (Table 2, Figure 5), ranging from 1.5:1 at E. Diamante to 32:1 in the deep Kasuga-2 plume. Fe:Mn ratios ≈32:1 were observed at Loihi Seamount [*Sedwick et al.*, 1992], presumably due to CO_2-weathering reactions between CO_2-rich fluids and the host basalts. Still higher Fe:Mn (54:1) were reported from Kilauea volcano, where lava flowing into the ocean resulted in the formation of acidic conditions and the complete dissolution of the basaltic matrix [*Resing and Sansone*, 2002]. Thus, depending on the reaction conditions, there are a wide range of possible relationships between Fe and Mn.

[30] Of the volcanoes observed here, Seamount X, Nikko, Daikoku, E. Diamante, and the shallow Kasuga-2 system all exhibit relatively low Fe:Mn ratios (Table 2, Figure 5). The shallow Kasuga-2 system was visited by *McMurtry et al.* [1993], where a low-temperature system with elevated alkalinity and CO_2 yielded a very low Fe:Mn ratio of 0.1:1, much lower than the 3:1 level observed

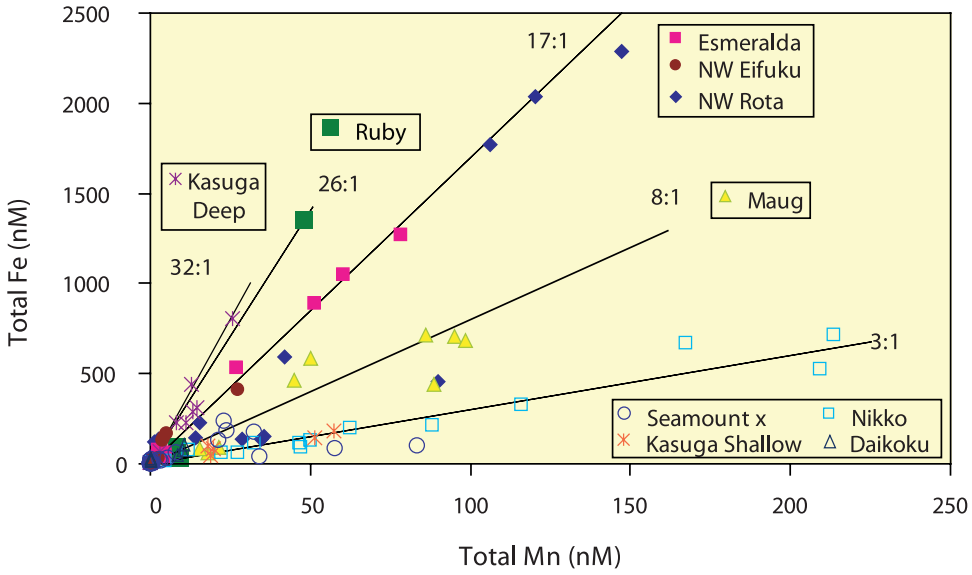

Figure 5. Total dissolvable Fe (TDFe) and total dissolvable Mn (TDMn) at each of the intensely active volcanoes.

here and also quite low compared with Loihi Seamount (32:1), which also had excess alkalinity and CO_2. Here the Kasuga-2 plume was also very rich in H_2S, having the highest values reported at any of the volcanoes in this study. In fact, the 13.2 μM H_2S reported here is higher than the 1.6 μM H_2S found in vent fluids by *McMurtry et al.* [1993] at the 39°C vent they sampled on the summit of Kasuga-2, suggesting that the venting is more robust now than when visited by *McMurtry et al.* [1993] or that they did not locate the most active sites of venting. The many-fold excess of H_2S relative to Fe suggests that Fe levels are likely reduced by the formation of Fe sulfide phases, thus producing the Fe:Mn observed here. Both Daikoku and Nikko had relatively elevated vent fluid temperatures [*Embley et al.*, 2007], suggesting that they mimic other high temperature systems with moderately low Fe:Mn. Seamount X was not well explored during ROV surveys and only low-temperature diffuse venting was found.

[31] Venting at Maug, Esmeralda, NW Eifuku, Kasuga-2 deep, Ruby, and NW Rota-1 had much higher Fe:Mn. At NW Rota-1 the high acidity of the fluids venting from the volcano likely dissolve the host rock, producing fluids with elevated Fe:Mn which are closer to those in the host rock [see *Resing et al.*, 2007]. Maug, Ruby, and Esmeralda show evidence of being high alkalinity/high CO_2 systems like Loihi, suggesting that elevated Fe levels come from carbonic acid dissolution of the host rocks. By contrast, the deep Kasuga-2 and NW Eifuku systems appear to have high CO_2 and no alkalinity, suggesting that the reaction path was either too short or reaction conditions were unfavorable to the formation of alkalinity. Liquid CO_2 droplets and CO_2-rich hydrothermal fluids were both venting from NW Eifuku and, as a result, there is a reasonable chance that the plume sample with the large CO_2 signal included either a droplet of liquid CO_2 or some of the CO_2 hydrate [see *Lupton et al.*, 2006]. This would result in a decoupling between hydrothermal "fluids" and CO_2 levels. In such a case, we may have a plume sample whose pH and CO_2 levels are the result of a droplet of pure CO_2, while the rest of the chemistry is represented by hydrothermal fluids with elevated Fe:Mn. The Fe:Mn in the deep Kasuga-2 plume is among the most elevated levels observed coming from a hydrothermal system and are matched only by those at Loihi [*Sedwick et al.*, 1992]. The type of venting might be similar to that at Loihi where elevated alkalinity was 2–4% of the CO_2. Here the absence of alkalinity in the plumes may be attributed to poor precision associated with small changes in pH and ΣCO_2 observed here.

5.3. CO_2 and ^{3}He

[32] ^{3}He comes almost entirely from mantle sources [*Craig and Lupton*, 1981], while CO_2 can come from other sources, including oceanic crust, sedimentary carbonates, and organic matter [*Poreda and Craig*, 1989; *Sano and Marty*, 1995]. The CO_2 observed at these arc volcanoes is greatly enriched compared with MORs [see *Resing et al.*, 2004], which likely reflects the input of this subducted carbon into arc volcanic systems [*Sano and*

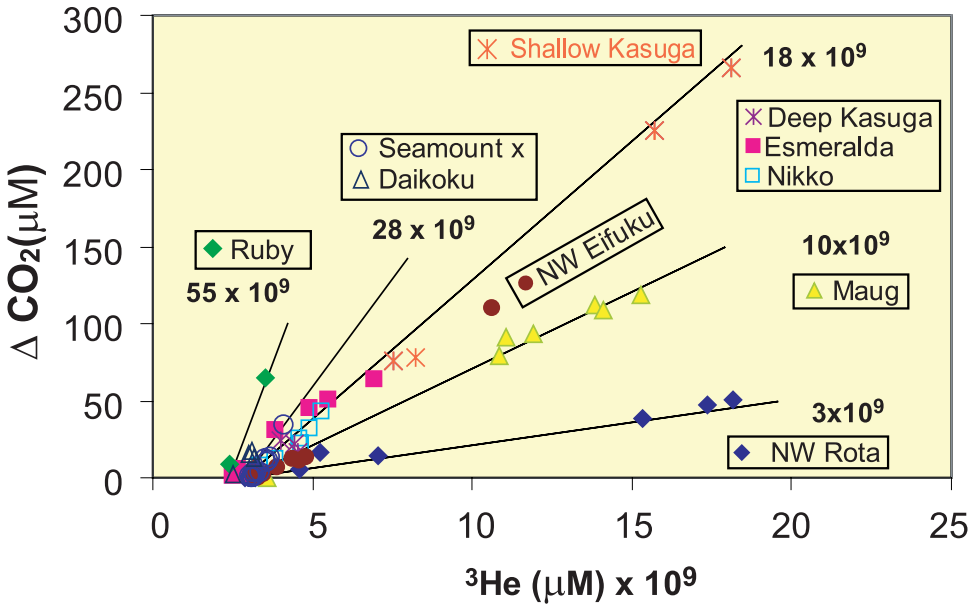

Figure 6. ΔCO_2 versus ^3He at the moderate-to-intensely active volcanoes along Mariana Arc. ΔCO_2 is the change in ΣCO_2 from that in the regional background.

Marty, 1995]. The CO_2:^3He observed at the different volcanoes here spans a wide range from 3 to 55 $\times$ 10^9 (Figure 6, Table 3). The lowest value observed here is 3.2 $\times$ 10^9 at NW Rota-1. This value is close to the global average for MOR fluids and basalt glasses of 1.9 $\pm$ 1.2 and 2.1 $\pm$ 0.6, respectively [*Resing et al.*, 2004, and references therein] and to the accepted value for the upper mantle (2 $\times$ 10^9). The highest value from Ruby (55 $\times$ 10^9) is among the highest values reported at either subaerial or submarine arc volcanoes and clearly reflects the addition of CO_2 into the volcanic hydrothermal system. *Sano and Marty* [1995] suggest that ratios above 2 $\times$ 10^9 arise from the input of CO_2 from the slab and that the relative contributions of CO_2 from the mantle and the slab can be calculated (Table 3). For example, at NW Rota-1 the percent of slab-derived carbon would be estimated to be 38%, while that at Ruby would be estimated to be >96%. After NW Rota-1, Maug has the next lowest CO_2:^3He of 10 $\times$ 10^9, suggesting that 80% of the CO_2 at Maug is from a slab source. Thus, the major source of CO_2 for all of the volcanoes, except for NW Rota-1, is the subducting slab.

[33] The generally accepted upper mantle helium isotope ratio R/R_a (where $R = {}^3He/{}^4He$ in a sample and $R_a = {}^3He/{}^4He$ in air) is 8.0 $\pm$ 1 [*Poreda and Craig*, 1989]. This is based on the value observed in MOR basalts and hydrothermal fluids. Arc helium is thought to be a mixture of helium from the melting of new mantle material and mobilization of He from the downgoing slab. The slab retains little of its original ^3He but contains sediments that are relatively richer in ^4He producing $R/R_a \approx 5$ to 7 at arc volcanoes [*Sano and Marty*, 1995]. Almost all of the volcanoes sampled here have R/R_a values that generally fall within the upper mantle range (Table 3). Although the lowest values (Seamount X, Esmeralda, and Nikko) are lower than 7, potentially placing them within Sano and Marty's arc helium range. The standard deviation of the R/R_a at those volcanoes places them within (or very close to) the accepted upper mantle value. Although there is clearly real variability in the R/R_a values beyond their standard deviations, it is difficult to assess the meaning of their distribution. The highest R/R_a (8.4 $\pm$ 1) is at NW Rota-1 where we suggested that most of the CO_2 came from the mantle; thus these two findings are consistent. However, the volcano with the largest CO_2:^3He and thus the greatest slab influence, Ruby, has an intermediate R/R_a (7.6 $\pm$ 0.6) that does not fall into the typical range for "arc helium." It seems likely that in general, the source of the He at these volcanoes is mostly from the mantle, with variable and poorly defined contributions from the slab. These observations are generally consistent with the few available data on the submarine arc with an R/R_a = 8.1 at Suiyo on the Izu-Bonin Arc [*Tsunogai et al.*, 1994], an R/R_a = 7.31 at NW Eifuku on the Mariana Arc [*Lupton et al.*, 2006], and a range of

R/R_a from 5.9 to 7.4 at Brothers Volcano on the Kermadec Arc (J. Lupton, unpublished data, 2008).

5.4. Hydrothermal Constraints on Magmatic Activity

[34] The wide range of hydrothermal activity encountered along the Mariana Arc is the result of many factors including source rock composition, the relative amounts of magmatic gasses, and ultimately the magmatic state of a given volcano. In this section, we examine the magmatic state as the primary factor in the hydrothermal activity and its variability. The ongoing eruption at NW Rota-1 in 2004 and 2006 [*Chadwick et al.*, 2008] establishes it as a magmatically robust end-member of the magmatic cycle. The full magmatic cycle likely involves the emergence of a magma chamber, eruption, and magma chamber collapse and/or cooling through the circulation of water through the hot rock. An important variable is that a receding front of magma leaves behind hot rock, while an emerging magma chamber releases magmatic products (CO_2, SO_2, etc.) into an older, colder volcanic edifice. Here we present a simple model of hydrothermal evolution based only on waning activity. Our limited geochemical and physical information allows for evaluating the data within this simple model, but interpreting these data within the context of an entire magmatic cycle would be overinterpretation.

[35] We consider NW Rota-1, which is in an eruptive state, to be at the beginning of the volcanic-hydrothermal cycle. It is characterized by the venting of magmatic volatiles SO_2 and CO_2, resulting in highly acidic fluids and bulk dissolution of the host rocks. The ability of the SO_2 (a strong acid) to escape the system and enter the ocean unreacted is evidence that the magma chamber is close to the surface of the volcano [*Resing et al.*, 2007]. In this magmatic state, the hydrothermal products escape into the ocean and are not deposited within the volcano. In these highly acidic fluids excess dissolved CO_2 as H_2CO_3 is favored over H^+ and HCO_3^-:

$$HCO_3^- + H^+ = H_2CO_2. \quad (4)$$

making the CO_2 unreactive with the surrounding rocks.

[36] When the eruptive phase ends, the front of molten material recedes due both to magma chamber collapse and cooling by fluid circulation. As the reaction path of the hydrothermal fluids lengthens, contact between water and rock increases causing fluid temperatures to rise. In addition, SO_2 reacts to form sulfur, sulfuric acid (equation (2)), and H_2S:

$$4\,SO_2 + 4\,H_2O = H_2S + 3H_2SO_4 \quad (5)$$

which can also react to form sulfur:

$$2\,H_2S + O_2 = 2S^0 + 2H_2O. \quad (6)$$

The sulfuric acid (equations (2) and (5)) is consumed through reaction with the host rocks. In this setting deposits of sulfates and elemental sulfur are formed within the volcano [e.g., *Binns et al.*, 1993]. Large deposits of elemental sulfur in both solid and liquid form were identified at Nikko and Daikoku volcanoes [*Embley et al.*, 2007]. The fluids exiting the volcano remain somewhat acidic and CO_2 remains undissociated. These fluids might be rich in Mg, SO_4^{2-}, H_2S, Fe, Mn, and potentially Al, as seen in the Manus Basin [*Gamo et al.*, 1997; *Resing et al.*, 2007]. The acidic conditions would suggest elevated Fe levels and a high Fe:Mn. Along the Mariana Arc, Kasuga-2, Nikko, and Daikoku fluids seem to fit this scenario. At these volcanoes, the changes in plume pH are mostly from CO_2 with some contribution of H^+. The deep plumes at Kasuga-2 have elevated Fe:Mn, while the shallow Kasuga-2, Daikoku, and Nikko fluids have low Fe:Mn but elevated H_2S, suggesting that Fe is being removed into sulfide phases, thereby decreasing the Fe:Mn. The extremely high Fe values at Nikko and in the deep Kasuga-2 plume are also consistent with acidic fluids, although the relatively low Fe values at Daikoku and shallow Kasuga-2 are somewhat inconsistent with this setting.

[37] As the magma chamber recedes the reaction path is further lengthened, H^+ is fully consumed, and more equilibrium-based high-temperature hydrothermal reactions dominate the fluid chemistry [e.g., *Bowers et al.*, 1988]. Although the pH rises, this type of hydrothermal fluid is still mildly acidic [e.g., *Butterfield et al.*, 2003] and CO_2 remains unreactive to the host rock. These fluids resemble high-temperature fluids in other settings, most notably the MORs, but with some excess sulfur as H_2S and elemental sulfur (equations (5) and (6)), and low-to-moderate Fe:Mn. Along the Mariana Arc, the plume chemistry above Seamount X appears to fit this category with moderate Fe levels and intermediate Fe:Mn.

[38] As the source of the magma deepens further, the reaction path is again lengthened. The high-temperature fluids mix with interstitial cold seawater and sulfides are deposited. The remaining acidity is consumed. The pH is high enough to allow the H_2CO_3 to dissociate (the reverse of equation (4)), and now the H^+ reacts with the host rock to produce alkalinity (equation (3)). This final scenario is similar to that at Loihi [*Sedwick et al.*, 1992] which has high CO_2, excess alkalinity, moderate pH, and $\pm H_2S$. Esmeralda Bank, Ruby, and Maug fit into this category, with each showing clear evidence of excess alkalinity (Figure 4 and Table 3) and large enrichments in CO_2 and Fe. The Fe:Mn in these fluids are variable, and lower than those at Loihi. This may be the result of temperature variability in the fluids and/or the removal of Fe from the fluids as Fe oxides or sulfides.

[39] As a volcano continues to age, less magmatic gas escapes, the edifice cools, and hydrothermal activity decreases. Volcanoes with the lowest activity, i.e., those in Table 4, fit into this category.

[40] East Diamante and NW Eifuku are more difficult to place within our model. East Diamante produced plumes rich in particulate elemental sulfur, intermediate levels of CO_2, but little Fe, Mn, and ^{3}He. The relationship between pH and CO_2 indicates that the source fluids were rich in CO_2 and alkalinity, suggesting the magmatic volatiles have reacted with the host volcanic rocks over a long path to generate alkalinity and any magmatic SO_2 was consumed deep within the volcano. As a result, the elemental sulfur must not arise from the disproportionation of SO_2 (equation (2)) but from other processes. It is unlikely that the sulfur was mobilized directly from a native sulfur deposit because sulfur is insoluble in both hot and cold water. The oxidation of H_2S to form S (equation (6)) is one possibility; however, a large hydrothermal source of H_2S is at odds with a plume without large concentrations of other hydrothermal species (^{3}He, Fe, and Mn). We hypothesize that the elemental S arises from the oxidation of metal sulfides within the volcanic edifice near the volcano-water interface:

$$2MeS + O_2 = 2MeO + 0.25\,S_8. \quad (7)$$

Sulfur is a well known intermediate of metal sulfide oxidation in inorganic processes [e.g., *Bouffard et al.*, 2006; *Nowak and Socha*, 2006; *Padilla et al.*, 2008] as well as during microbially catalyzed oxidation of metal sulfides by acidophilic bacteria [e.g., *Schippers and Sand*, 1999]. This sulfur has been found to coat the surfaces of metal sulfides and form discrete particles that are $\sim$2-μm diameter [*Bouffard et al.*, 2006]. Our data are limited and a more detailed exploration of this volcano would be required to validate this hypothesis.

[41] NW Eifuku discharged highly CO_2-rich fluids, with abundant Fe and an elevated Fe:Mn. The extremely high CO_2 concentrations were reflected by the presence of CO_2 clathrates and the venting of liquid CO_2 at the summit of the volcano [*Lupton et al.*, 2006] and suggests an abundant source of magmatic gasses. The absence of mineral acidity, and therefore magmatic SO_2, suggests that the source of these gasses resides at a depth that allows the SO_2 to react within the volcano. In contrast, the CO_2 did not react to form alkalinity over this longer reaction path, perhaps inhibited by cooler reaction temperatures. These data suggest that the magma chamber at NW Eifuku may reside deep within the volcano and the magmatic gasses rise into an older, colder substrate. The abundance of gasses suggests that this magma chamber is emerging rather than decaying.

6. Conclusions

[42] There is clear and abundant evidence of hydrothermal activity at 16 submarine volcanoes along the Mariana Arc from 13.5°N to 23.2°N. Two additional volcanoes, NW Uracas and W. Diamante, had marginal evidence for hydrothermal activity, but further surveys are required before positively identifying them as being hydrothermally active. Six of the volcanoes had very small hydrothermal signals, suggesting fairly weak or diffuse activity. However, it should be noted that three of these volcanoes were surveyed with single hydrocasts and that additional surveying might find more intense plumes. The other 10 active volcanoes had much stronger plume signals. In some cases this might be due to a fortuitous placement of the hydrocast, but in most cases the hydrothermal activity was so pervasive that it would likely have been observed regardless of the exact placement of the hydrocast. One example of the importance of hydrocast location is Ruby, where hydrothermal activity was not found during the 2003 survey, but was found on a different tow track in 2006.

[43] The chemistry of the fluids venting from individual volcanoes could be characterized for the 10 volcanoes with the largest plume signals. The compositions of the plumes varied widely

from volcano to volcano. Particulate matter in the plumes ranged from mostly pFe at Esmeralda Bank, Ruby, Maug, and the deep Kasuga-2 plume, to mostly pS at E. Diamante, Shallow Kasuga-2, and Daikoku, to a mix of pFe, pAl, and pS at NW Rota-1. Changes in pH were caused by the addition of SO_2, CO_2, and alkalinity, indicating several different effects: (1) the juvenile hydrothermal venting rich in magmatic volatiles at NW Rota-1, (2) deep-seated hydrothermal systems with excess CO_2 expressed as both CO_2 gas and alkalinity, and (3) systems with changes in pH brought about mostly by CO_2. All of the volcanoes except NW Rota-1 had elevated CO_2:^{3}He with respect to upper mantle source values, indicating that 80% (Maug) to 96% (Ruby) of the CO_2 venting from these volcanoes has a slab source. By contrast, the He isotopic composition of the fluids in the plumes indicates that most of the ^{3}He is derived from the upper mantle. It is possible that the ^{3}He and ^{4}He in the crust (if any) might be liberated from the slab at shallower depths and lower temperatures while the CO_2, present as both organic carbon and carbonate, is released at greater depths and temperatures and is thus released from the slab after the He.

[44] The 10 volcanoes can be placed within a generalized model based on the relative location of the magma chamber within the volcano. Where the magmatic source was closest to the surface of the volcano, acidic fluids (SO_2) rich in CO_2 were vented, as was observed for NW Rota-1, Kasuga-2, Nikko, and Daikoku. As the distance between the magmatic source and the surface of the volcano increases, most of the acid is consumed and fluids rich in CO_2 are emitted from the volcano (Seamount X). Eventually, the distance between the magmatic source and the volcano's surface is so large that all of the magmatic SO_2 is consumed, the pH rises, and weathering reactions predominate, producing fluids with elevated alkalinity and CO_2, which is consistent with the fluids coming from Esmeralda, Maug, and Ruby.

[45] The results of the study of the submarine volcanoes along the Mariana Arc are important for a variety of reasons related to their impact on the surrounding ocean and the flux of chemical components into the oceans. The elevated CO_2:^{3}He suggest that previous calculations [e.g., *Resing et al.*, 2004] of CO_2 flux from submarine volcanoes to the oceans based on MORs and arcs [*Marty and Tolstikhin*, 1998], must be revised upward. The extraordinarily elevated levels of Fe, Mn, and Al from these volcanoes suggest that the shallow summits of some of these volcanoes may impact biological activity by providing micronutrients to the oceans on a local scale.

Acknowledgments

[46] Carbon dioxide measurements were made by PMEL's CO_2 group. Methane analyses were made by A. Graham. Editorial assistance was provided by R. Whitney. Special thanks to the captain and crew of the R/V *Thomas Thompson.* The maps used here were produced by S. Merle at the Newport, Oregon PMEL. This work was funded by NOAA Office of Exploration, the PMEL Vents program, and the Joint Institute for the Study of the Atmosphere and Oceans. This is PMEL publication 3186 and JISAO publication 1469.

References

Baker, E. T., R. W. Embley, S. L. Walker, J. A. Resing, C. E. J. de Ronde, G. J. Massoth, and K.-I. Nakamura (2008), Hydrothermal activity and volcano distributions along the Mariana Arc, *J. Geophys. Res.*, *113*, B08S09, doi:10.1029/2007JB005423.

Binns, R. A., et al. (1993), Hydrothermal oxide and gold-rich sulfate deposits of the Franklin Seamount, Western Woodlark Basin, Papua New Guinea, *Econ. Geol.*, *88*, 2122–2153.

Bloomer, S. H., R. J. Stern, E. Fisk, and C. H. Geschwind (1989), Shoshonitic Volcanism in the Northern Mariana Arc: 1. Mineralogic and major and trace element characteristics, *J. Geophys. Res.*, *94*, 4469–4496, doi:10.1029/JB094iB04p04469.

Bouffard, S. C., B. F. Divera-Vasquez, and D. G. Dixon (2006), Leaching kinetics and stoichiometry of pyrite oxidation from a pyrite-marcasite concentrate in acid ferric sulfate media, *Hydrometallurgy*, *84*, 225–238, doi:10.1016/j.hydromet.2006.05.008.

Bowers, T. S., A. C. Campbell, C. I. Measures, A. J. Spivack, M. Khadem, and J. E. Edmond (1988), Chemical controls on the composition of vent fluids at 13°–11°N and 21°N, East Pacific Rise, *J. Geophys. Res.*, *93*(B5), 4522–4536, doi:10.1029/JB093iB05p04522.

Butterfield, D. A., W. E. Seyfried Jr., and M. D. Lilley (2003), Composition and evolution of hydrothermal fluids, in *Energy and Mass Transfer in Submarine Hydrothermal Systems*, *Dahlem Workshop Rep.*, vol. 89, edited by P. E. Halbach, V. Tunnicliffe, and J. Hein, pp. 123–161, Free Univ. of Berlin, Berlin.

Chadwick, W. W., Jr., K. V. Cashman, R. W. Embley, H. Matsumoto, R. P. Dziak, C. E. J. de Ronde, T. K. Lau, N. D. Deardorff, and S. G. Merle (2008), Direct video and hydrophone observations of submarine explosive eruptions at NW Rota-1 Volcano, Mariana Arc, *J. Geophys. Res.*, *113*, B08S10, doi:10.1029/2007JB005215.

Cowen, J. P., G. J. Massoth, and R. A. Feely (1990), Scavenging rates of dissolved manganese in a hydrothermal vent plume, *Deep-Sea Res.*, *37*(10), 1619–1637, doi:10.1016/0198-0149(90)90065-4.

Craig, H., and J. Lupton (1981), Helium-3 and mantle volatiles in the ocean and the ocean crust, in *The Sea*, vol. 7, *The Oceanic Lithosphere*, edited by C. E. Emiliani, pp. 391–428, John Wiley, New York.

de Ronde, C. E. J., E. T. Baker, G. J. Massoth, J. E. Lupton, I. C. Wright, R. A. Feely, and R. G. Greene (2001), Intra-oceanic subduction-related hydrothermal venting, Kermadec volcanic arc, New Zealand, *Earth Planet. Sci. Lett.*, *193*, 359–369, doi:10.1016/S0012-821X(01)00534-9.

de Ronde, C. E. J., G. J. Massoth, E. T. Baker, and J. E. Lupton (2003), Submarine hydrothermal venting related to volcanic arcs, *Soc. Econ. Geol. Spec. Publ.*, *10*, 91–110.

de Ronde, C. E. J., et al. (2007), Submarine hydrothermal activity along the mid-Kermadec arc, New Zealand: Large-scale effects on venting, *Geochem. Geophys. Geosyst.*, *8*, Q07007, doi:10.1029/2006GC001495.

Dixon, T. H., R. Batiza, K. Futa, and D. Martin (1984), Petrochemistry, age and isotopic composition of alkali basalts from Ponape Island, Western Pacific, *Chem. Geol.*, *43*, 1–28, doi:10.1016/0009-2541(84)90138-4.

Embley, R. W., E. T. Baker, W. W. Chadwick Jr., J. E. Lupton, J. A. Resing, G. J. Massoth, and K. Nakamura (2004), Explorations of Mariana Arc volcanoes reveal new hydrothermal systems*Eos Trans. AGU*, *85*(4), 37, 39.

Embley, R. W., et al. (2006), Long-term eruptive activity at a submarine arc volcano, *Nature*, *441*(7092), 494–497, doi:10.1038/nature04762.

Embley, R. W., et al. (2007), Exploring the submarine ring of fire: Mariana Arc- Western Pacific, *Oceanography*, *20*, 68–79.

Feely, R. A., G. J. Massoth, and G. T. Lebon (1991), Sampling of marine particulate matter and analysis by x-ray fluorescence spectrometry, in *Marine Particles: Analysis and Characterization*, *Geophys. Monogr. Ser.*, vol. 63, edited by D. C. Hurd and D. W. Spencer, pp. 251–257, AGU, Washington, D. C.

Fryer, P., J. B. Gill, and M. C. Jackson (1997), Volcanologic and tectonic evolution of the Kasuga seamounts, northern Mariana Trough: Alvin submersible investigations, *J. Volcanol. Geotherm. Res.*, *79*, 277–311, doi:10.1016/S0377-0273(97)00013-9.

Fryer, P., H. Fujimoto, M. Sekine, L. E. Johnson, J. Kasahara, H. Masuda, T. Gamo, T. Ishii, M. Ariyoshi, and K. Fujioka (1998), Volcanoes of the southwestern extension of the active Mariana island arc: New swath-mapping and geochemical studies, *Isl. Arc*, *7*, 596–607, doi:10.1111/j.1440-1738.1998.00212.x.

Gamo, T., et al. (1993), Revisits to the mid-Mariana Trough hydrothermal site and discovery of new venting in the southern Mariana region by the Japanese submersible Shinkai 6500, *InterRidge News*, *2*(1), 11–14.

Gamo, T., K. Okamura, J.-L. Charlou, T. Urabe, J.-M. Auzende, J. Ishibashi, K. Shitashima, and H. Chiba (1997), Acidic and sulfate-rich fluids from the Manus back-arc basin, Papua New Guinea, *Geology*, *25*, 139–142, doi:10.1130/0091-7613(1997)025<0139:AASRHF>2.3.CO;2.

Gamo, T., et al. (2004), Discovery of a new hydrothermal venting site in the southernmost Mariana Arc: Al-rich hydrothermal plumes and white smoker activity associated with biogenic methane, *Geochem. J.*, *38*, 527–534.

Govindaraju, K. (1989), 1989 compilation of working values and sample description for 272 geostandards, *Geostand. Newsl.*, *13*, 1–113, doi:10.1111/j.1751-908X.1989.tb00476.x.

Ishibashi, J., and T. Urabe (1995), Hydrothermal activity related to arc-backarc magmatism in the western Pacific, in *Backarc Basins: Tectonics and Magmatism*, edited by B. Taylor, pp. 451–495, Plenum, New York.

Kadko, D. C., N. D. Rosenberg, J. E. Lupton, R. W. Collier, and M. D. Lilley (1990), Chemical reaction rates and entrainment within the Endeavour Ridge hydrothermal plume, *Earth Planet. Sci. Lett.*, *99*, 315–335, doi:10.1016/0012-821X(90)90137-M.

Kelley, D. S., M. D. Lilley, J. E. Lupton, and E. J. Olson (1998), Enriched H-2, CH4, and He-3 concentrations in hydrothermal plumes associated with the 1996 Gorda Ridge eruptive event, *Deep Sea Res., Part II*, *45*, 2665–2682, doi:10.1016/S0967-0645(98)00088-5.

Lewis, E., and D. Wallace (1998), Program developed for CO_2 system calculations, *ORNL/CDIAC-105*, Carbon Dioxide Inf. Anal. Cent., U. S. Dept. of Energy, Oak Ridge, Tenn.

Lupton, J., et al. (2006), Submarine venting of liquid carbon dioxide on a Mariana Arc volcano, *Geochem. Geophys. Geosyst.*, *7*, Q08007, doi:10.1029/2005GC001152.

Luther, G. W., III, B. T. Glazer, L. Hohmann, J. I. Popp, M. Taillefert, T. F. Rozan, P. J. Brendel, S. M. Theberge, and D. B. Nuzzio (2001), Sulfur speciation monitored in situ with solid state gold amalgam voltametric microelectrodes: Polysulfides as a special case in sediments, microbial mats and hydrothermal vent waters, *J. Environ. Monit.*, *3*, 61–66, doi:10.1039/b006499h.

Martinez, F., and B. Taylor (2003), Controls on back-arc crustal accretion: Insights from the Lau, Manus and Mariana basins, in *Intra-Oceanic Subduction Systems: Tectonic and Magmatic Processes*, edited by R. D. Larter and P. T. Leat, *Geol. Soc. London Spec. Publ.*, *219*, 19–54.

Marty, B., and I. N. Tolstikhin (1998), CO_2 fluxes from mid-ocean ridges, arcs, and plumes, *Chem. Geol.*, *145*, 233–248, doi:10.1016/S0009-2541(97)00145-9.

Massoth, G. J., E. T. Baker, R. A. Feely, J. E. Lupton, R. W. Collier, J. F. Gendron, K. K. Roe, S. M. Maenner, and J. A. Resing (1998), Manganese and iron in hydrothermal plumes resulting from the 1996 Gorda Ridge Event, *Deep Sea Res., Part II*, *45*(12), 2683–2712, doi:10.1016/S0967-0645(98)00089-7.

Massoth, G. J., C. E. J. de Ronde, J. E. Lupton, R. A. Feely, E. T. Baker, G. T. Lebon, and S. M. Maenner (2004), The chemically rich and diverse submarine hydrothermal plumes of the southern Kermadec volcanic arc (New Zealand), in *Intra-Oceanic Subduction Systems: Tectonic and Magmatic Processes*, edited by R. D. Larter and P. T. Leat, *Geol. Soc. London Spec. Publ.*, *219*, 119–139.

Massoth, G. J., et al. (2007), Multiple hydrothermal sources along the south Tonga arc and Valu Fa Ridge, *Geochem. Geophys. Geosyst.*, *8*, Q11008, doi:10.1029/2007GC001675.

Masuda, H., R. A. Lutz, S. Matsumoto, S. Masumoto, and K. Fujioka (1994), Topography and geochemical aspects on the most recent volcanism around the spreading axis of the southern Mariana Trough at 13°N, *J. Deep-Sea Res.*, *10*, 176–185.

McMurtry, G. M., P. N. Sedwick, P. Fryer, D. L. Vonderhaar, and H. W. Weh (1993), Unusual geochemistry of hydrothermal vents on submarine arc volcanoes: Kasuga Seamounts Northern Mariana Arc, *Earth Planet. Sci. Lett.*, *114*, 517–528, doi:10.1016/0012-821X(93)90080-S.

Measures, C. I., J. C. Yuan, and J. Resing (1995), Determination of iron in seawater by flow injection analysis using in-line preconcentration and spectrophotometric detection, *Mar. Chem.*, *50*, 3–12, doi:10.1016/0304-4203(95)00022-J.

Millero, F. J. (1979), The thermodynamics of the carbonate system in seawater, *Geochim. Cosmochim. Acta*, *43*, 1651–1661, doi:10.1016/0016-7037(79)90184-4.

Nowak, P., and R. P. Socha (2006), Oxidation and dissolution of metal sulfides from flotation wastes in circulating water-

the fate of sulfide sulfur, *Physiochem. Problems Mineral Proc.*, *40*, 135–148.

Padilla, R., P. Pavez, and M. C. Ruiz (2008), Kinetics of copper dissolution from sulfidized chalcopyrite at high pressure in H_2SO_4-O_2, *Hydrometallurgy*, *91*, 113–120, doi:10.1016/j.hydromet.2007.12.003.

Peacock, S. M. (1990), Fluid processes in subduction zones, *Science*, *248*, 329–337, doi:10.1126/science.248.4953.329.

Peate, D. W., and J. A. Pearce (1998), Causes of spatial compositional variations in Mariana Arc lavas: Trace element evidence, *Isl. Arc*, *7*, 479–495, doi:10.1111/j.1440-1738.1998.00205.x.

Poreda, R., and H. Craig (1989), Helium Isotope ratios in Circum Pacific volcanic arcs, *Nature*, *338*, 473–478, doi:10.1038/338473a0.

Resing, J. A., and M. J. Mottl (1992), Determination of manganese in seawater by flow injection analysis using online preconcentration and spectrophotometric detection, *Anal. Chem.*, *64*, 2682–2687, doi:10.1021/ac00046a006.

Resing, J. A., and F. J. Sansone (2002), The chemistry of lava-seawater interactions II: The elemental signature, *Geochim. Cosmochim. Acta*, *66*(11), 1925–1941, doi:10.1016/S0016-7037(01)00897-3.

Resing, J. A., J. E. Lupton, R. A. Feely, and M. D. Lilley (2004), CO_2 and ^3He in hydrothermal plumes: Implications for Mid-Ocean Ridge CO_2 flux, *Earth Planet. Sci. Lett.*, *226*, 449–464, doi:10.1016/j.epsl.2004.07.028.

Resing, J. A., E. T. Baker, G. Lebon, R. W. Embley, W. W. Chadwick Jr., J. E. Lupton, and G. J. Massoth (2007), Venting of acid-sulfate fluids in a high-sulfidation setting at NW Rota-1 submarine volcano on the Mariana Arc, *Econ. Geol.*, *102*(6), 1047–1061, doi:10.2113/gsecongeo.102.6.1047.

Sabine, C. L., R. M. Key, and M. Hall (1999), Carbon dioxide, hydrographic, and chemical data obtained during the R/V *Thomas G. Thompson* cruise in the Pacific Ocean (WOCE section P10, October 5–November 10, 1993), *NDP-071*, *Carbon Dioxide Inf. Anal. Cent.*, Oak Ridge, Tenn.

Sakamoto-Arnold, C. M., K. S. Johnson, and C. L. Beehler (1986), Determination of hydrogen sulfide in seawater using flow injection analysis and flow analysis, *Limnol. Oceanogr.*, *31*(4), 894–900.

Sano, Y., and B. Marty (1995), Origin of carbon in fumarolic gas from island arcs, *Chem. Geol.*, *119*, 265–274, doi:10.1016/0009-2541(94)00097-R.

Schippers, A., and W. Sand (1999), Bacterial leaching of metal sulfides proceeds by two indirect mechanisms via thiosulphate or via polysulfides and sulfur, *Appl. Environ. Microbiol.*, *65*, 319–321.

Sedwick, P. N., G. M. McMurtry, and J. D. Macdougall (1992), Chemistry of hydrothermal solutions from Pele's vents, Loihi Seamount, Hawaii, *Geochim. Cosmochim. Acta*, *56*, 3643–3667, doi:10.1016/0016-7037(92)90159-G.

Stern, R. J., and L. D. Bibee (1984), Esmeralda Bank: Geochemistry of an active submarine volcano in the Mariana Island Arc, *Contrib. Mineral. Petrol.*, *86*, 159–169, doi:10.1007/BF00381843.

Stern, R. J., S. H. Bloomer, P.-N. Lin, and N. C. Smoot (1989), Submarine arc volcanism in the southern Mariana Arc as an ophiolite analogue, *Tectonophysics*, *168*, 151–170, doi:10.1016/0040-1951(89)90374-0.

Stern, R. J., N. Basu, E. Kohut, J. Hein, and R. W. Embley (2004), Petrology and geochemistry of igneous rocks collected in association with ROV investigations of three hydrothermal sites in the Mariana Arc: NW Rota-1, E Diamante, and NW Eifuku, *Eos Trans. AGU*, *85*(47), Fall Meet. Suppl., Abstract V43F-07.

Stern, R. J., Y. Tamura, R. W. Embley, O. Ishizuka, S. Merle, N. K. Basu, H. Kawabata, and S. H. Bloomer (2008), Evolution of West Rota Volcano, an extinct submarine volcano in the Southern Mariana Arc: Evidence from sea floor morphology, remotely operated vehicle observations, and ^{40}Ar-^{39}Ar geochronological studies, *Isl. Arc*, *17*, 70–89.

Stüben, D., et al. (1992), First results of study of sulphur-rich hydrothermal activity from an island-arc environment: Esmeralda Bank in the Mariana Arc, *Mar. Geol.*, *103*, 521–528, doi:10.1016/0025-3227(92)90037-I.

Tsunogai, U., J. Ishibashi, H. Wakita, T. Gamo, K. Watanabe, T. Kajimura, S. Kanayama, and H. Sakai (1994), Peculiar features of Suiyo Seamount hydrothermal fluids, Izu-Bonin Arc: Differences from subaerial volcanism, *Earth Planet. Sci. Lett.*, *126*, 289–301, doi:10.1016/0012-821X(94)90113-9.

U. S. Department of Energy (1994), *Handbook of Methods for the Analysis of the Various Parameters of the Carbon Dioxide System in Sea Water, Version 2, ORNL/CDIAC-74*, edited by A. G. Dickson and C. Goyet, Washington, D. C.

van der Hilst, R., R. Engdahl, W. Spakman, and G. Nolet (1991), Tomographic imaging of subducted lithosphere below northwest Pacific island arcs, *Nature*, *353*, 37–42, doi:10.1038/353037a0.

Venzke, E., , R. W. Wunderman, L. McClelland, T. Simkin, J. F. Luhr, L. Siebert, G. Mayberry, and S. Sennert (Eds.) (2002), *Global Volcanism, 1968 to the Present*, *Global Volcanism Progr. Digital Inf. Ser.*, vol. GVP-4, Smithson. Inst., Washington, D. C. (Available at http://www.volcano.si.edu/reports/)

Walker, S. L., E. T. Baker, J. A. Resing, W. Chadwick, G. T. Lebon, J. E. Lupton, and S. M. Merle (2008), Eruption-fed particle plumes and volcaniclastic deposits at a submarine volcano: NW Rota-1, Mariana arc, *J. Geophys. Res.*, *113*, B08S11, doi:10.1029/2007JB005441.

Woodhead, J. D. (1989), Geochemistry of the Mariana Arc (western Pacific): Source compositions and processes, *Chem. Geol.*, *76*, 1–24, doi:10.1016/0009-2541(89)90124-1.

Young, C., and J. E. Lupton (1983), An ultratight fluid sampling system using cold-welded copper tubing, *Eos Trans. AGU*, *64*, 735.